Geochemistry, Geophysics, Geosystems®

RESEARCH ARTICLE
10.1029/2023GC010994

Key Points:

- Large magmatic dike intruded within carbonates of the southern Apennines
- Tectonic extension played a pivotal role in magma uprise and volcanism along graben-bounding faults
- Tectonic horst uplift is likely coeval with the caldera phase of Roccamonfina volcano

Supporting Information:

Supporting Information may be found in the online version of this article.

Correspondence to:

J. Natale,
jacopo.natale@uniba.it

Citation:

Natale, J., Vitale, S., Giordano, G., Fedele, L., Lucci, F., Vona, A., et al. (2023). The Taverna San Felice dike (NE of Roccamonfina volcano): Unraveling magmatic intrusion processes and volcano-tectonics in the Tyrrhenian margin of the southern Apennines. *Geochemistry, Geophysics, Geosystems*, *24*, e2023GC010994. https://doi.org/10.1029/2023GC010994

Received 11 APR 2023
Accepted 20 JUL 2023

Author Contributions:

Conceptualization: Jacopo Natale, Stefano Vitale, Guido Giordano
Data curation: Jacopo Natale, Stefano Vitale, Lorenzo Fedele, Federico Lucci, Alessandro Vona, Ernesto Paolo Prinzi, Francesco D'Assisi Tramparulo
Funding acquisition: Stefano Vitale
Investigation: Jacopo Natale, Stefano Vitale, Guido Giordano, Ernesto Paolo Prinzi, Francesco D'Assisi Tramparulo

The Taverna San Felice Dike (NE of Roccamonfina Volcano): Unraveling Magmatic Intrusion Processes and Volcano-Tectonics in the Tyrrhenian Margin of the Southern Apennines

Jacopo Natale[1,2], Stefano Vitale[1,2,3], Guido Giordano[4], Lorenzo Fedele[1], Federico Lucci[2], Alessandro Vona[4], Ernesto Paolo Prinzi[1], Francesco D'Assisi Tramparulo[1], Roberto Isaia[3], and Sabatino Ciarcia[5]

[1]Dipartimento di Scienze della Terra, dell'Ambiente e delle Risorse (DiSTAR), Università di Napoli Federico II, Napoli, Italy, [2]Dipartimento di Scienze della Terra e Geoambientali, Università degli Studi di Bari Aldo Moro, Bari, Italy, [3]Istituto Nazionale di Geofisica e Vulcanologia, sezione di Napoli Osservatorio Vesuviano, Napoli, Italy, [4]Dipartimento di Scienze, Università di Roma Tre, Roma, Italy, [5]Dipartimento di Scienze e Tecnologie, Università degli Studi del Sannio, Benevento, Italy

Abstract The Roccamonfina volcano is located within the Garigliano Graben (southern Apennines, Italy) and has been active throughout the Middle-Late Pleistocene. Along its polyphase volcanic history (630–55 ka), including several caldera-forming eruptions (385–230 ka), several effusive/mildly explosive monogenetic events occurred along the volcano slopes, within the summit caldera, and along the graben-bounding carbonate reliefs. In this paper, we present a multidisciplinary study of a mafic magmatic feeder dike intruded within the Meso-Tertiary carbonates and overlying Lower Pleistocene breccias of Mt Cesima, northeast of the Roccamonfina volcano. We performed a stratigraphic and structural survey of the area and petrographic analyses on several samples of the dike. Results indicate that a ∼1 km long fissure fed an eruption that also emplaced a Strombolian pyroclastic sequence. Petrological data show that an open-system mafic recharge fueled the tephritic magma that fed the eruption, whereas no evidence of significant pre/syn-eruptive assimilation of carbonate has been identified. Stratigraphic and petrological data do not allow to firmly constrain the timing of the eruption, which could belong both to the pre-Brown Leucitic Tuff (>354 ka) and to the post-White Trachytic Tuffs (<230 ka) epochs of activity of the Roccamonfina volcano. Structural data show that the dike is broadly oriented E-W and changes direction toward NE-SW in correspondence with a pre-existing fault damage zone. We suggest that magma was intruded during an N-S trending extensional event in the Middle Pleistocene, whose prolonged activity resulted in regional uplift and exhumation of regional significance.

1. Introduction

Volcanism worldwide occurs largely in extensional settings, including oceanic ridges, continental rifts, and synorogenic back-arc basins, where tectonic conditions favor magma ascent (e.g., Favela et al., 2000; Galindo & Gudmundsson, 2012; Goldberg, 2010; Gudmundsson, 1990, 1992). In areas of stretched crust, volcanic activity can produce different kinds of structures, including fissure ramparts, scoria cones and vent alignments (e.g., Cardello et al., 2020; De Matteo et al., 2018; Ruch et al., 2016; Smets et al., 2015; Smith & Németh, 2017; Tibaldi et al., 2020; Trippanera et al., 2018, 2019). However, understanding the relationships between volcanism and tectonics over time may be challenging, especially in areas where different volcanic and tectonic phases have occurred.

Such is the case of the Pleistocene Italian volcanism, which is localized along the eastern margin of the Tyrrhenian Sea, a back-arc basin resulting from the subduction of the Adria lithosphere beneath the Sardinia-Corsica block since at least the Serravallian (Vitale & Ciarcia, 2013 and references therein). The back-arc opening-related extension progressively moved following the thrust front migration toward NE/E in the southern Apennines and SE/S in the Calabria-Peloritani Terrane (Carminati et al., 2014; Faccenna et al., 1996; Vitale & Ciarcia, 2013, and references therein). Up to the Early Pliocene, the orogenic construction was dominantly driven by thin-skinned tectonics with flat-lying thrust faults separating the major thrust sheets. Thereafter, the axial part of the southern

Methodology: Jacopo Natale, Stefano Vitale, Guido Giordano, Lorenzo Fedele, Federico Lucci, Alessandro Vona
Project Administration: Stefano Vitale, Sabatino Ciarcia
Software: Jacopo Natale
Supervision: Stefano Vitale, Guido Giordano, Roberto Isaia, Sabatino Ciarcia
Validation: Jacopo Natale, Stefano Vitale, Guido Giordano, Lorenzo Fedele
Visualization: Jacopo Natale, Lorenzo Fedele, Federico Lucci
Writing – original draft: Jacopo Natale, Stefano Vitale
Writing – review & editing: Jacopo Natale, Stefano Vitale, Guido Giordano, Lorenzo Fedele, Federico Lucci, Alessandro Vona, Ernesto Paolo Prinzi, Francesco D'Assisi Tramparulo, Roberto Isaia, Sabatino Ciarcia

Apennines experienced an out-of-sequence thrusting phase, which led to the formation of ramp-dominate thrusts that also involved the wedge-top basin deposits (Cardello et al., 2021; Vitale et al., 2020). As a result, extensional tectonics affected the Tyrrhenian margin of the southern Apennines since the Early Pleistocene (Alessandri et al., 2021; Bergomi et al., 1969; De Rita & Giordano, 1996; Giordano et al., 1995; Ippolito., 1973; Nicotera & Civita, 1969). This produced many structural highs and depressions between the Lazio and Campania regions (Figure 1a), hosting the volcanoes of the Roman and Campanian Provinces (e.g., Peccerillo, 2017), also in the present-day offshore (Conte et al., 2020). Among the structural depressions, the most significant is the Campania Plain, hosting the Campi Flegrei, Ischia, and Somma-Vesuvius active volcanoes (Figure 1a). Further to the north, the Roccamonfina volcano developed within the Garigliano Graben.

This extensional phase is testified by NW-SE and NE-SW faults in the whole southern Apennines chain, including the Garigliano and Campania plains and the Neapolitan volcanoes (Boncio et al., 2016; Bosi & Giordano, 1997; Caiazzo et al., 2006; Ciaranfi et al., 1983; Cinque et al., 2000; De Rita & Giordano, 1996; Galderisi et al., 2017; Tramparulo et al., 2018; Vitale & Isaia, 2014).

Geochemical and petrological features of volcanic products indicate that the extensional tectonics drove their emplacement (Di Girolamo et al., 1988; Lustrino et al., 2011; Peccerillo, 2017). However, knowledge of the structural mechanisms that acted during the early establishment of the Pleistocene volcanic activity in central-southern Italy, and the interplay between volcanism and tectonics through time still needs to be investigated thoroughly (e.g., Cardello et al., 2020; Giordano et al., 1995; Isaia et al., 2019; Natale et al., 2022; Tramparulo et al., 2018; Vitale et al., 2019).

Furthermore, the emplacement of magmatic dikes within carbonate rock has drawn the attention of several researchers since the magma-carbonate interaction may explain significant explosivity during Plinian eruptions (e.g., Somma-Vesuvius; Buono et al., 2020; Jolis et al., 2013, 2015; Knuever et al., 2023). However, the feeding system is usually poorly exposed, often only in strongly exhumed fossil systems (e.g., Iceland, Oman), or not exposed at all, limiting the possibility to investigate dike emplacement mechanisms within homogeneous or faulted country rocks. In addition, the behavior of a dike within preexisting fault-zones (Gudmundsson, 2011, 2020), its intrusion mechanisms (Mode I and/or II-III), magma flow patterns (Koopmans et al., 2022), and near-surface contact geometries (Poppe et al., 2020) which may affect surface deformation and faulting patterns (Trippanera et al., 2015), still have room for further comprehension, especially in sedimentary host-rocks.

In this work, we deepen these topics as we conducted a multidisciplinary investigation of a magmatic dike and the eruptive fissure system a few km northeast of the Roccamonfina volcano in the Taverna San Felice (TSF) quarry (Figure 1), previously not documented in the literature. This structure represents a unique, beautifully exposed example in the whole Pleistocene Italian volcanic area of a dike hosted in Meso-Quaternary rocks and may provide interesting clues on the relationships between the formation of the Garigliano Graben and the peripheral volcano-tectonic activity related to the Roccamonfina volcano.

2. Geological Setting

Roccamonfina volcano is located within the Garigliano Graben, straddling the Roman and Campanian magmatic provinces (Conticelli et al., 2010; Peccerillo, 2017). These include the volcanic districts of Vulsini (0.9–0.12 Ma), Vico (0.9–0.095 Ma), Sabatini (0.6–0.09 Ma), Colli Albani (0.7–0.03 Ma), Ernici/Middle Latin Valley/Volsci Volcanic Field (0.76–0.23 Ma), Roccamonfina (0.63–0.05 Ma), Ischia (0.2 Ma-active), Campi Flegrei (0.08 Ma-active) and Somma-Vesuvius (0.3 Ma-active) (Figure 1a), all classically ascribed to a subduction-related potassic to ultra-potassic post-collisional volcanism (Di Girolamo & Morra, 1988; Peccerillo, 2017).

The eruptive history of the Roccamonfina volcano consists of three main periods (Conticelli et al., 2009). During the first stage (630–400 ka), large volumes (about 100 km^3) of lava and small-volume ignimbrites were emplaced, building the ancient stratovolcano (Tedesco, 1965), along with smaller phonolitic domes and scoria cones erupted along NE-SW regional lineaments (Bosi, 1994; De Rita & Giordano, 1996; Di Girolamo, 1972, Di Girolamo et al., 1991; Sgrosso & Aiello, 1963). Some of these vents are located within the surrounding Mesozoic carbonate ridges, including the Taverna San Felice, Presenzano ($^{40}Ar/^{39}Ar$ age of 600 ± 3 ka, Ballini et al., 1989) and Sesto Campano eruptive centers on the Mt. Cesima ridge (Figure 1), and the vent reported on the northern slope of Mt Massico (Servizio Geologico d'Italia, 1968). The products of this period are K-rich and strongly silica-undersaturated, belonging to the so-called High-Potassic series (HKS; Appleton, 1972; "plagioclase

10.1029/2023GC010994

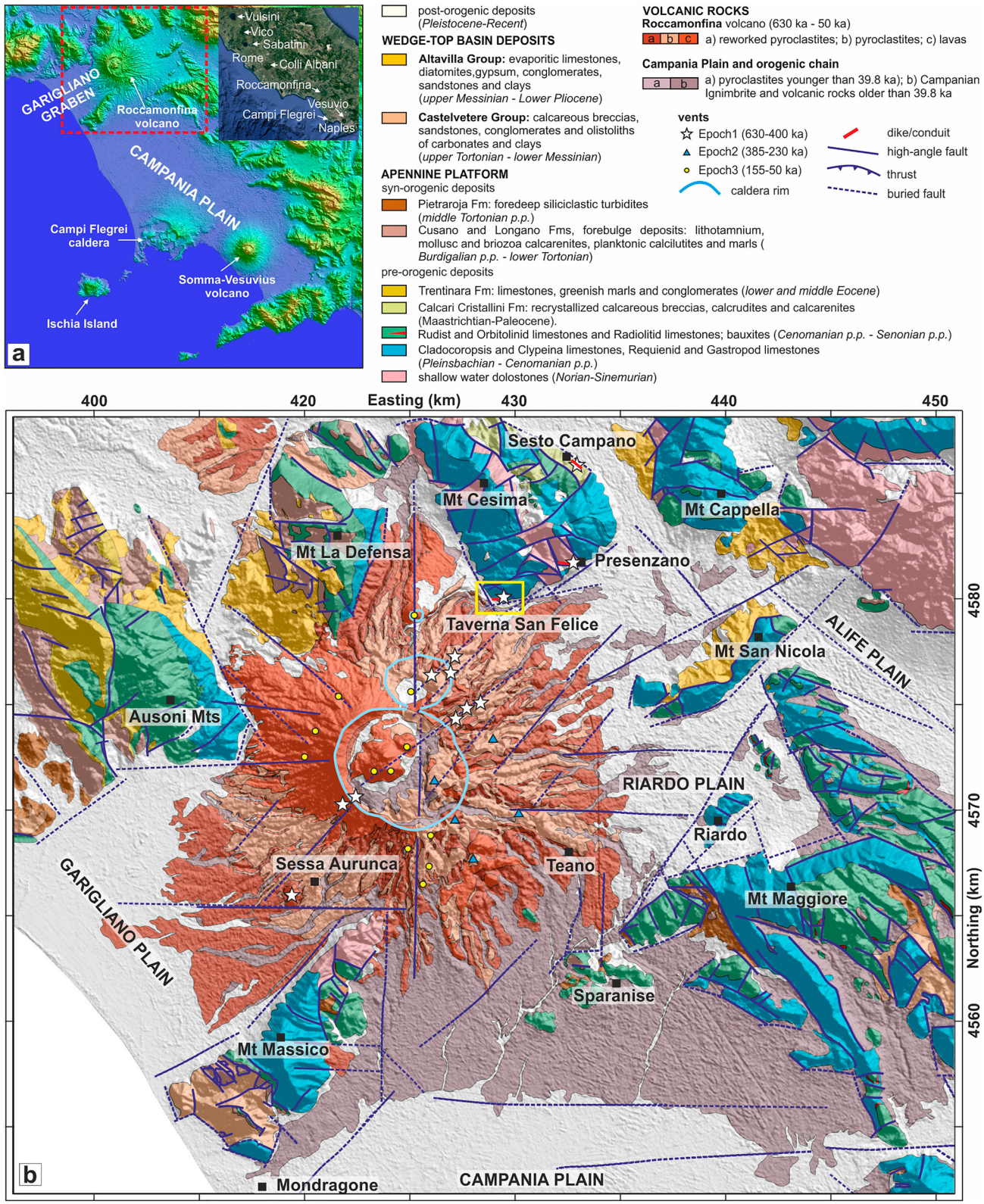

Figure 1. (a) Digital Elevation Model (DEM) of the Campania Plain-Garigliano Graben area extracted from ALOS3D DEM (Japan Aerospace Exploration Agency, 2021), with the inset at the upper right highlighting the volcanic districts of the Roman and Campanian magmatic provinces of central-southern Italy and the red dashed rectangle showing the position of panel (b). (b) Geological map of the Garigliano Graben (modified after Vitale & Ciarcia, 2018), the yellow box indicates the study area.

leucitites," Conticelli et al., 2009). In this phase also, some Plinian phonolitic-to-trachytic activity is reported, such as the Rio Rava eruption, dated at ~440 ka (K/Ar; Rouchon et al., 2008) and 437 ka ($^{40}Ar/^{39}Ar$; Russo Ermolli et al., 2010), and other recognized in the distal record, dated at ~426 ka (Amato et al., 2014).

The second period (385–230 ka) was characterized by the emplacement of the Brown Leucitic Tuff (BLT, 354 ka), an ignimbrite sequence with leucite-bearing pumice clasts (De Rita & Giordano, 1996; Luhr & Giannetti, 1987; Rouchon et al., 2008). The eruption produced a collapse of the volcano edifice toward the NE and marked the transition to a slightly silica-undersaturated magmatism (the KS Potassic series; Appleton, 1972; "shoshonites," SHO, Conticelli et al., 2009). Subsequent Plinian paroxysmal activity emplaced the White Trachytic Tuffs sequence (WTTs, 310–230 ka; Ballini et al., 1989; Cole et al., 1993; De Rita & Giordano, 1996; De Rita et al., 1998; Giannetti, 1990; Giannetti & Luhr, 1983; Giordano, 1998), and the deposits of the Yellow Trachytic Tuff eruption (YTT), which produced the northern caldera, dated at 227 ka (Cole et al., 1992; Giannetti, 1996; Luhr & Giannetti, 1987).

During the third period (155–50 ka), the Roccamonfina volcano mainly emplaced effusive products, fed by subalkaline magmas (HKCA, high-K calcalcaline series), including the summit dome of Monte Santa Croce (Conticelli et al., 2009). The variable serial affinity displayed by the products emplaced during the three periods of activity was ascribed to partial melting of a heterogeneous mantle, with the HKS magmas being sourced from different domains with respect to the KS and HKCA ones (Conticelli et al., 2009; Peccerillo, 2017). The volcanic successions of the Roccamonfina volcano are capped by the deposits of the Campanian Ignimbrite eruption (dated at 39.8 ka; Giaccio et al., 2017), originated from the Campi Flegrei caldera, ~60 km to the southeast.

The study area (yellow box, Figure 1b) is located within the NE-SW trending Garigliano Graben, a structural depression bounded by Meso-Cenozoic carbonate ridges to SW (Mt Massico), SE (Mt Maggiore), NW (Aurunci Mts), N (Mt La Defensa) and NE (Mt Cesima). The latter is constituted by pre-orogenic shallow-water Triassic-Cretaceous carbonates and, locally, by Eocene and Early-to-Middle Miocene limestones (Vitale & Ciarcia, 2018). The southern part of Mt Cesima consists of a carbonate succession, including Cretaceous shallow-water limestones passing upward to Maastrichtian-Paleocene recrystallized calcarenites and breccias (Calcari Cristallini Fm; Vitale & Ciarcia, 2022). The succession is folded, forming a south-verging anticline, and displaced by Lower-Pleistocene normal faults with associated syn-extensional continental deposits (D'Agostino et al., 1998; Demangeot, 1965). The pyroclastic products of the Roccamonfina volcano and the Campanian Ignimbrite eruption, as well as Volturno river deposits (Valente et al., 2019), contributed to the filling of the Garigliano Graben, formed starting from the Early Pleistocene (Giordano et al., 1995; Figure 1b). NE-SW major high-angle faults, and subordinate NW-SE faults, bound the tectonic depression. Younger E-W and N-S faults crosscut the carbonate ridges around the graben and the Roccamonfina edifice (e.g., De Rita & Giordano, 1996).

3. Materials and Methods

3.1. Field and Unmanned Aerial Vehicle (UAV) Stratigraphic and Structural Survey

The investigated magmatic dike was studied in the active cement quarry of TSF. Since 2019, we have carried out numerous geological surveys of the area following the progress of the excavation activities, which gradually exposed new stratigraphic sections, which include pyroclastic deposits from the Roccamonfina, and proximal Strombolian pyroclastic successions associated with the feeder dike. Concerning the structural features, we measured fault and fracture attitudes in the exposed sections of the dike, associated products, and host rock. Fault data, including fault plane and striation orientations, and kinematics, were processed with Tectonics FP (Reiter & Acs, 1996-2020) and Open Stereo (Open Stereo Softwre Package, 2018) open-source software. In addition, for sites inaccessible to in situ measurements and to preserve records of the outcrops during the progress of excavations, we performed Unmanned Aerial Vehicle (UAV)-based photogrammetric surveys from September 2020 to January 2022. The UAV images were acquired using a DJI Mavic Air 2 UAV with a 1/2″ CMOS 12 MP sensor and 24 mm-equivalent focal length, with 4:3 aspect ratio in the 12 MP camera configuration to maximize the pixel resolution. The average front and side overlap of the pictures is around 80%, with acquisition angles between nadiral and 30°, following the best practices for UAV surveys (James & Robson, 2012; Stroner et al., 2021; USGS, 2017).

The aerial images captured by UAV were processed and used to build photogrammetric Virtual Outcrop Models with Agisoft Metashape Pro software (Ver 1.5.1). The 3D texturized models were exported in .kmz format and

imported within GeoVis3D Open software (GeoVis3D, 2022) to extract planar and linear structural data using the best-fit plane and lineation measuring mode, respectively, and finally exported in .csv format for structural analysis purposes.

3.2. Petrographic and Whole-Rock Geochemical Analyses of the Volcanic Products

Rock samples were collected from the dike and the associated volcanic deposits (see below) for a total of 11 samples. Magmatic fabric and primary mineral assemblages were investigated on polished thin sections both at the polarizing microscope and at the Scanning Electron Microscope (SEM), using a Field Emission Scanning Electron Microscope Zeiss Gemini Sigma 300, hosted at the Laboratorio Interdipartimentale di Microscopia Elettronica (LIME), Roma Tre University. Back-scattered electron images were collected using a high-definition back-scattered electron detector (HDBSD), and the composition of mineral phases was qualitatively investigated using a Bruker XFlash 6,160 Energy Dispersive X-ray Spectroscopy (EDS) detector. Operating conditions were 15 keV and up to 20 nA for a working distance ranging from 7 to 8.5 mm, and aperture size up to 60 mm. EDS-spectra were normalized to the peak of Si (Pulses/eV) to highlight chemical zoning. Whole-rock geochemical analyses were performed at the DiSTAR laboratories. Samples were cut with a diamond-blade circular saw, crushed in a steel jaw-crusher, washed in deionized water, dried out, hand-picked to remove the most altered external portions, and finally pulverized in a low-blank agate mill. Rock powders were used to produce pressed powder pellets, analyzed for major- and trace elements by XRF (X-ray fluorescence) spectrometry using a Panalytical Axios instrument. Analytical uncertainties are in the order of 1%–2% for major elements, 5%–10% for trace elements. Weight loss on ignition was determined gravimetrically after heating rock powders (pre-dried at ~150°C overnight) at 950°C for 4 hr. Full results and sample locations are reported in Supporting Information S1 (Table S1).

4. Results

4.1. Main Features of the Study Area

In the TSF quarry, excavation operations have been active since 1981 and have progressively exposed a large magmatic dike for a length of over 250 m. The TSF dike crops out in the central part of the quarry, with an E-W orientation at its base and a NE-SW direction from the middle toward the topmost outcrops (Figure 2a).

The dike thickness ranges between 5 and 28 m (Figure 2b), with smaller values in the lower part of the quarry where the dike dips by ca. 65° toward NNW and many apophyses are also exposed (Figures 2c and 2d), with both lateral tips exposed. The carbonate host rocks (Figure 2c) show a thermo-metamorphic aureole that is better developed in the lower part of the quarry. Along the contacts, polished fault planes (Figure 2e) with kinematic indicators (Figure 2f) occur parallel to the dike-host rock contact. The host rocks are highly damaged by fractures and faults, making bedding planes barely recognizable (Figure 2g). Nevertheless, relics of sedimentary features allow them to be identified as part of the Lower Cretaceous oolitic lithostratigraphic unit.

Faults (Figure 2h) are visible as polished surfaces (Figure 2j) or as finer grained cataclastic bands (Figure 2i). Carbonate speleothems and pseudo-karst features are frequent, as in the nearby outcrops on the Mt Cesima ridge (Figure 2o). In the nearby abandoned quarry, to the NW of the active one (Figure 2a), the bedding planes are instead visible, steeply dipping toward the south (Figure 2n), with numerous high-angle faults with a similar planar attitude (Figure 2n). Sedimentary indicators allow recognition that the stratigraphic polarity is normal (Figure 2p). The TSF dike hosts pervasive joints (Figure 2k), faults (Figure 2l), and related shear fractures (Figure 2m), with the contact between the TSF dike and the host rock changing significantly along its length (Figure 2b). A sharp contact aureole, 1–4 m thick, occurs along the boundary between the dike and the cataclastic limestones (Figure 3a). Where the dike intrudes the Lower Pleistocene breccia (Figure 3c), the margins are irregular and blunt (Figure 3d), with no evident contact aureole. In the lower section of the quarry, apophyses, locally enclosed in the host rock (Figure 3b), vary in length between 2 and 7 m, with an average thickness of 0.8 m, pinching out toward the tips. The tips of finger-like apophysis can vary from wedge-like to rounded (Figures 3e and 3f). Some of them show staircase-like sharp contacts (Figure 3e). Frequently, host rock enclaves are observed within the dike along the dike-host rock margin (Figures 3g and 3i). Locally, sub-vertical peperite-like dikes, filled by reddish-scoria lapilli coated by a carbonate matrix, occur (Figure 3j). Dike failed-paths (horns) occur both as a partial (soft-linked) linkage with isolated bridges (i.e., sections of wall-rock connecting on the two sides of a dike,

10.1029/2023GC010994

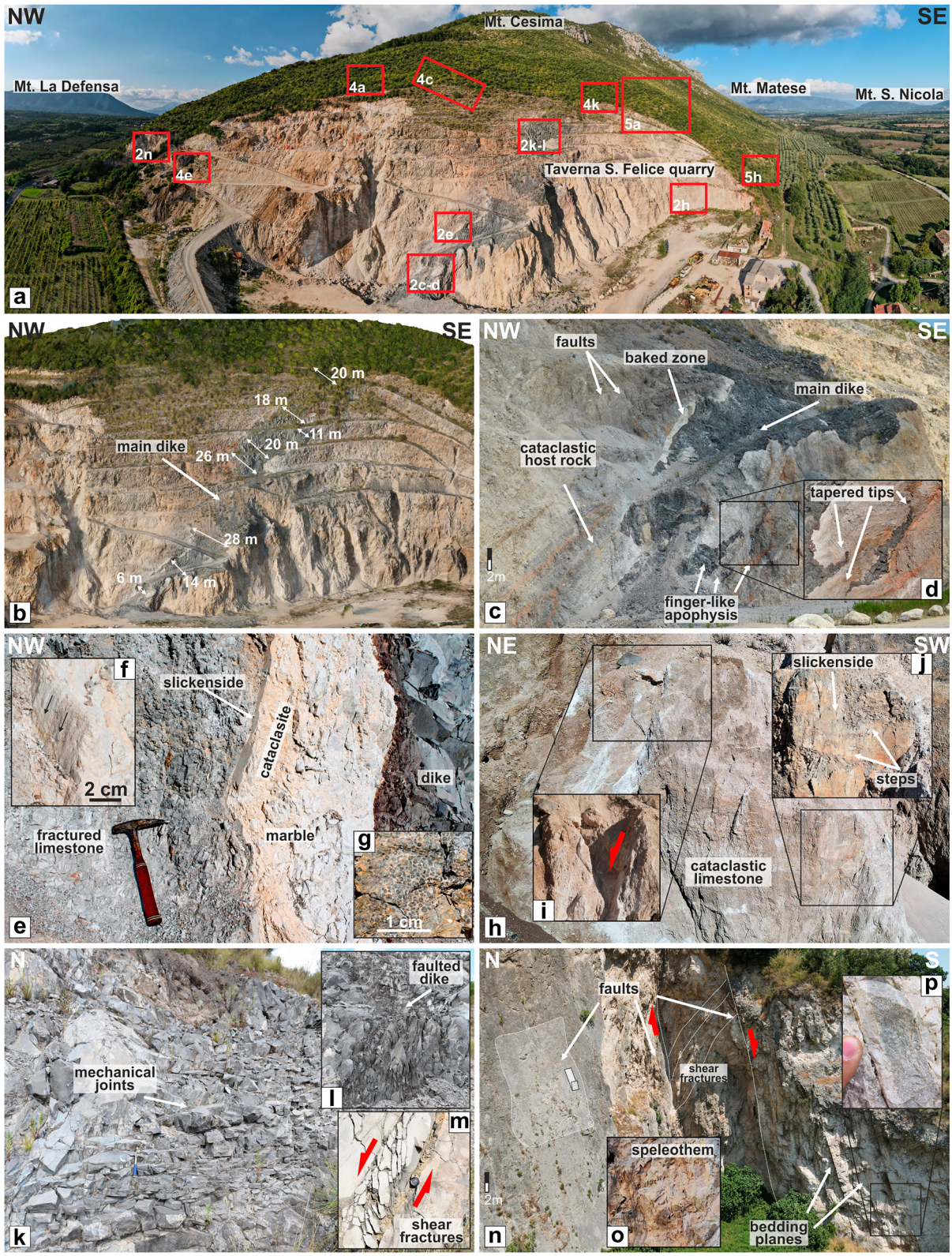

Figure 2.

Figure 3h) or as complete linkage (hard-linked) in which a section of the wall rock is isolated within a dike lens between overlapping segments (Figure 3k).

4.2. Stratigraphic Survey

Within the topmost part of the quarry (Figures 4a and 4b), an up to 15 m thick Strombolian pyroclastic succession, mostly preserved in the hanging-wall of normal faults (Figures 4c), was observed to lay on altered pyroclastic deposits, in turn, laying on cataclastic Cretaceous limestones and Lower Pleistocene breccia deposits. The altered sequence starts with a ~2 m thick pedogenized reddish pyroclastic material topped by a 60 cm thick, variably altered, clast-supported, white-to-gray clast-supported pumice lapilli layer (Figure 4a). This is covered in turn by a 1.6 m thick reworked and altered pyroclastic layer, which transitions upward to a mature reddish paleosol (Figures 4a and 4f). On top of this sequence, three main Strombolian eruptive units were observed (Units 1, 2, and 3; Figures 4j and 4k). Unit 1 varies in thickness between 2 and 5 m (Figures 4a and 4f), and is characterized by stratified to diffusely stratified scoria lapilli beds with interspersed fluidal bombs, dense scoria, lava, and carbonate ballistic clasts (in upward decreasing order of abundance). Unit 2 is a 5–6 m thick massive deposit made up of agglutinated scoria lapilli and spatter clasts, with ballistic ejecta made up of dense scoriae, lava, and carbonate clasts (Figures 4d, 4e, and 4j). The thickness reaches a maximum of 10 m in the most preserved sections (Figures 4c and 4g). Unit 3 is a clast-supported, very-coarse ballistic-rich unit composed of lava, large fluidal bombs, and carbonate clasts up to 1 m in diameter. Clasts of Unit 3 are extensively covered by a reddish oxidation patina.

The entire Strombolian succession is cut by faults and fractures, the latter frequently coated by carbonate-rich filling/patina (Figure 4) and mostly oriented parallel or obliquely to the excavation fronts (Figure 4). In the upper east corner of the quarry (Figure 5a), we report the occurrence of welded deposits made up of scoriaceous spatter clasts and scoria lapilli, over 2 m in thickness (Figures 5b and 5c). The distribution of these ramparts (Figure 5a) follows the same orientation of the uppermost portion of the dike. Several scattered outcrops of welded lapilli and spatter clasts (Figures 5d–5g), locally passing laterally to lava flow deposits (Figures 5h and 5i), are also present.

4.3. Structural Survey

The stereographic projections of the deformation structures are shown in Figure 6. The poles of the TSF dike boundaries (Figure 6a) form a cluster indicating a 324/56 mean plane. The rose diagram of map lineaments carried out on UAV-derived nadiral-view orthomosaic indicates preferred E-W and NE-SW directions, with the former mainly observed in the lowermost part of the quarry, the latter in the topmost (Figure 6b). At greater detail, E-W portions are connected by NE-SW segments in a left-stepping en-echelon fashion (Figure 6m). Fractures hosted in the TSF dike (Figure 6c) show two main clusters of the poles, indicating mean 223/62 and 202/82 planes. The joint direction highlighted in the rose diagram (Figure 6d) shows dominant NE-SW and secondary WNW-ESE directions. Poles to fractures within the host rock (Figure 6e) show two clusters with 085/82 and 119/62 mean planes. The rose diagram (Figure 6f) indicates the main N-S and a secondary NE-SW direction. The bedding attitude of the limestones is barely visible within the quarry and was measured in the nearby abandoned quarry, with high-angle south-dipping attitudes (Figure 6g). The TSF Strombolian pyroclastic units dip at around 40° toward SW, following the slope angle (Figure 6h).

Faults with different orientations affect the pyroclastic deposits (Figure 6i). The dominant fault directions are shown in the rose diagram (Figure 6j), showing dominant NE-SW and subordinate N-S and E-W directions. The latter crosscut the succession at the base of the TSF Strombolian deposits, recording greater displacements. We recognized two main fault systems, both made up of two fault sets. The first, named S1, is characterized by a NE-SW direction with conjugate planes and a few NW-SE directions, with dominant normal and subordinate

Figure 2. (a) Unmanned Aerial Vehicle (UAV) wide-angle picture of the Taverna San Felice quarry showing the study area, with red boxes highlighting the zoomed sections. (b) Texturized UAV photogrammetric 3D model of the quarry documenting dike thickness measurements along its visible strike. (c) Field photograph taken broadly parallel to the dike strike in its basal portion, where it is hosted in a cataclastic limestone showing a contact aureole. (d) Zoomed photo showing an isolated apophysis with both lateral tips showing tapered edges. (e–g) Zoomed field photographs showing the contact aureole of (c) and the polished fault planes. (h) UAV picture indicating some North-dipping E-W normal faults (j), and NE-SW normal faults (i). (k) Severe jointing in the medial part of the dike showing further faulting and fracturing (l and m). (n) UAV photo taken in the nearby abandoned quarry showing the nearly vertical South-dipping limestone beds affected by both E-W and NE-SW faults. (o) Field picture of one of the numerous examples of speleothems/pseudo-karst feature. (p) Field picture showing a fining upward oolitic bed. Enlarged inset photographs are presented in Supporting Information S1 (Figures S5 and S6).

10.1029/2023GC010994

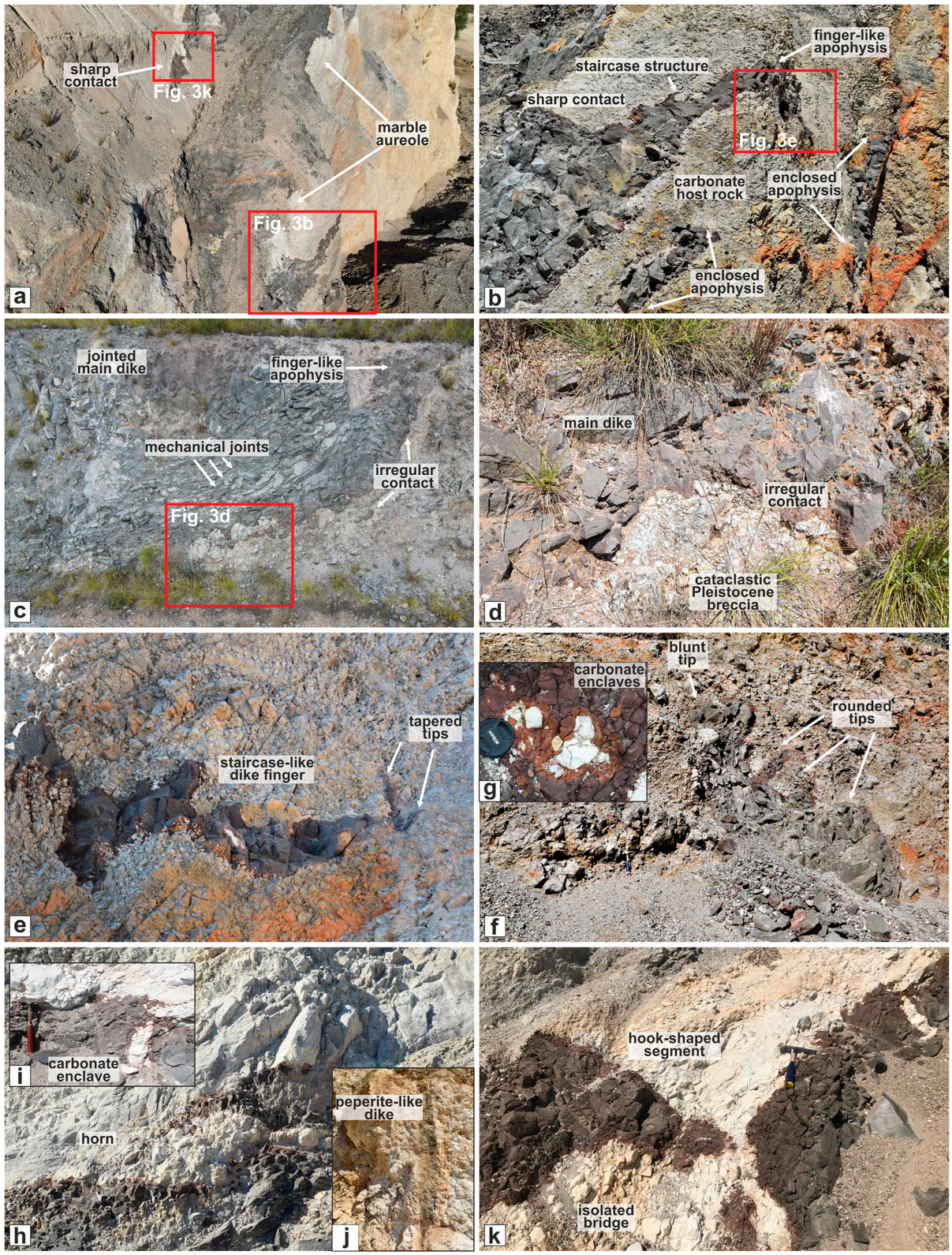

Figure 3.

transtensive kinematics (Figure 6k). The second, labeled S2 (Figure 6l), includes normal and transtensive faults that indicate dominant E-W and subordinate N-S directions. We also investigated the thickness distribution of the dike along its strike within the host rock in the exposed section (Figures 6m and 6n). Measurements were collected orthogonal to the dike boundaries with a regular step of ∼1.5 m along the strike (Figure 6m), corrected for the average dike dip (65°) to account for the apparent thickness. The elevation of the midpoint ranges between 5 and 80 m above the quarry base (orange points in Figure 6m, solid orange line in Figure 6n), with thickness ranging from ∼5 to 25 m (black dashed line; Figure 6n). The dashed blue box indicates the position of the intersection between the E-W and NE-SW fault zones. Reference to the corresponding host rock lithology is also indicated in the topmost part of Figure 6n.

4.4. Petrography

Host rock samples collected close to the contact with the TSF dike include both partially recrystallized limestones with relict oolites (Figure 7a) and completely recrystallized isotropic granoblastic marbles with abundant fluid inclusions (Figure 7b). Samples from the TSF feeder dike were collected in the core, along the dike/host-rock interface and from some apophyses. The samples from the dike core are weakly/moderately porphyritic (phenocrysts <15 vol%), poorly vesiculated lithic-free and microcrystalline, with a holocrystalline fine-grained groundmass (Figures 7c–7f). The alignment of clinopyroxene phenocrysts and microcrysts (and of plagioclase laths) defines a fluidal magmatic fabric (Figure 7e). Compared with the dike core samples, the samples from the dike margin display a higher vesicularity up to 30 vol% (Figure 7c), a less evident fluidal fabric and an oxidized reddish-brownish groundmass (Figure 7d). The primary assemblage is the same for the core and margin sample, composed of zoned euhedral clinopyroxene (Cpx), elongated platy plagioclase (Pl), euhedral to subhedral leucite (Lct), and opaque minerals (Opq). Rare nepheline and olivine microcrysts also occur, invariably showing interstitial growth texture in the groundmass (Figures S3 and S4 in Supporting Information S1). A very rare occurrence of brown mica is reported as inclusion at cores of clinopyroxene phenocrysts (Figure S3b in Supporting Information S1). Two different types of clinopyroxene crystals were observed (Figure S4 in Supporting Information S1). The Cpx1 type is represented by phenocrysts and groundmass microcrysts showing evident concentric reverse zoning, with yellow-to-green rounded cores (i.e., "green-core," gc) mantled by colorless rims. They are, in turn, covered by outer greenish rims that show equilibrium growth with groundmass plagioclase laths (Figure S3 in Supporting Information S1). The second clinopyroxene type Cpx2 population is light-green homogeneous microcrystals in groundmass (Figure 7g).

The juvenile clasts making up the Strombolian deposits (Units 1, 2, and 3) are represented by scoria lapilli and spatter clasts, both being weakly porphyritic (phenocrysts <20 vol%), moderately vesiculated (vesicles up to 30–40 vol, %), lithic-free and with a microcrystalline to hypohyaline fine-grained isotropic groundmass (Figures 7j and 7k). Oxidized reddish groundmass is locally observed. The primary assemblage consists of leucite, plagioclase, clinopyroxene (similar to the Cpx1 type from the dike samples) and opaque minerals (Figure S3 in Supporting Information S1).

The gray-to-white TSF pumice lapilli layer is made of weakly porphyritic (phenocrysts < 5 vol%), highly vesiculated (>60 vol, %) pumice clasts. Rare sanidine phenocrysts are set into a holohyaline groundmass (Figure 7l).

4.5. Whole-Rock Geochemistry

Rock samples were collected from the main dike, two from its core (PR8 and PR9), one from the margin, close to the contact with the host rock (PR1), and two from two apophyses (PR6 and PR7). Additional samples include

Figure 3. (a) Unmanned Aerial Vehicle (UAV) oblique view of the main body of the Taverna San Felice dike, showing the sharp contact with the host rock at the base of the quarry. (b) UAV picture of the upper part of the dike, hosted in the Pleistocene breccia, with a well-developed jointing and an irregular contact. (c) Finger-like and enclosed apophysis with rounded to tapered tips. (d) Zoomed field photograph of the irregular dike-host rock contact within the Pleistocene breccia. (e, f) Close-up views of the dike terminations, showing significant differences between cataclastic limestone and Lower Pleistocene breccia country rocks, resulting in sharp staircase-like contacts and wedge-like tips in the lower part of the quarry, and irregular contacts and rounded tips in an embedded apophysis in the upper part of the quarry, respectively. (g) Close-up view picture of calcinated carbonate enclaves with a reddish oxidized aureole. (h) "Horn," incomplete dike linkage between overlapping segments almost isolating a carbonate enclave raft. (i) Zoomed field photograph showing a large carbonate enclave raft within the dike. (j) Sub-vertical peperite-like dike, made-up of vesiculated and oxidized scoriae in a fluidized fine-lapilli carbonate-coated scoriae matrix crosscutting the cataclastic host rock. (k) Almost linked hook-shaped magma segment enclosing a carbonate bridge. Outcrop locations are given in Figure 2a. Enlarged inset photographs are presented in Supporting Information S1.

10.1029/2023GC010994

Figure 4.

two composite scoria clast samples (PR2 and PR3, from TFS Units 1 and 2, respectively), one spatter clast (PR4) and one bomb (PR5) from Unit 3 and a composite pumice lapilli sample (PP-PR) from the TSF pumice lapilli layer. The investigated samples were plotted on various classification and binary diagrams (Figure 8, and Figures S1 and S2 in Supporting Information S1), along with literature samples from the Roccamonfina volcano, distinguished in "pre-BLT" samples older than the BLT eruption (BLT, ~350 ka), including Rio Rava samples (~440 ka), BLT samples, "post-BLT" samples younger than the BLT (385–155 ka) and WTT (White Trachytic Tuffs, 310–230 ka) samples and the peripheral vents to the N and NE of the volcano edifice.

All dike samples are remarkably homogenous in composition, showing a strongly silica-undersaturated potassium-rich phonotephritic composition covering a very narrow compositional spectrum for all the major oxides (e.g., 49.2–49.5 wt% SiO_2, 17.7–18.1 wt% Al_2O_3, 3.08–3.37 wt% MgO, 6.59–6.99 wt% K_2O) and trace elements (e.g., 281–304 ppm Rb, 2,101–2,175 ppm Sr, 214–219 ppm Zr).

Samples from the TSF Strombolian deposit are mostly similar to the dike samples, showing a relatively homogeneous phonotephritic composition (e.g., 48.9–49.2 wt% SiO_2, 17.3–18.8 wt% Al_2O_3, 3.12–3.41 wt% MgO, 6.61–6.85 wt% K_2O, 330–474 ppm Rb, 2,159–2,202 ppm Sr, 221–224 ppm Zr). One single sample from the bottom of the sequence (Unit 1) clearly stands out, showing a slightly less evolved basanitic/tephritic composition (e.g., 46.1 wt% SiO_2, 16.9 wt% Al_2O_3, 4.63 wt% MgO, 5.93 wt% K_2O, 271 ppm Rb, 1757 ppm Sr). Both the dike and the Strombolian deposit samples are comparable with literature samples from the peripheral vents (which include also less evolved, MgO-richer compositions from the Sesto Campano and Presenzano locations; Figure 1b) and are in line with the pre-BLT products of the Roccamonfina activity, though with generally higher CaO at given MgO content.

The sample from the TSF pumice lapilli layer shows a trachyte composition and a slightly silica-undersaturated potassic affinity (e.g., 61.4 wt% SiO_2, 21.7 wt% Al_2O_3, 0.23 wt% MgO, 7.92 wt% K_2O, 497 ppm Rb, 267 ppm Sr, 540 ppm Zr). The composition is consistent with the literature data for the Roccamonfina activity younger than the BLT eruption (Figure 8), being overall comparable with the composition of the samples from the WTT eruptions. However, the compositional field of the WTT, also overlaps with the composition of some pre-BLT poorly recognized eruptions for whom only a few geochemical data are available, including Rio Rava eruption (Rouchon et al., 2008) and the slightly younger pre-BLT eruption recognized in the distal record (i.e., MOL13 tephra in Amato et al. (2014); not plotted in Figure 8 since no whole rock data is available).

5. Discussion

5.1. The Origin and Tectonic Significance of the TSF Dike

Several examples of peripheral monogenetic activity, accompanying the volcanic history of the Roccamonfina, are reported (e.g., De Rita & Giordano, 1996). Volcanic centers and dikes were also observed in the surrounding calcareous massifs bounding the Garigliano Graben, including; (a) the Presenzano fissure (Sgrosso & Aiello, 1963), (b) the Sesto Campano remnant, (c) a dike encountered in an aque duct gallery (Di Girolamo, 1972; Di Girolamo et al., 1991), (d) the scattered outcrops of lavas and scoria deposits at TSF (Di Girolamo et al., 1991), and (e) the vent reported on the northern slope of Mt Massico (Servizio Geologico d'Italia, 1968). Based on the petrological similarities with the pre-BLT Roccamonfina rocks, these centers were ascribed to the early activity (Epoch 1; 600–400 ka) by Di Girolamo et al. (1991). In this work, we envisage that these vents might have been fed by a common, regional-wide source, unrelated with the main stratovolcano, as corroborated by several geometric elements. In fact, structural data suggest that the orientation of the minimum stress (σ_3) at the time of intrusion was broadly N-S trending, with the E-W oriented dike, that is, ~45° from the respective radial direction from the volcano and dipping toward the north (Figure 9a). This suggests an origin from beneath the Mt. Cesima ridge and/or the former plain (Figure 9b) instead of a radial dike or a cone sheet propagating from beneath the

Figure 4. (a) Field photograph showing the pumice lapilli layer (highlighted in the zoomed section) embedded within a thick pedogenized pyroclastic sequence overlain by the Taverna San Felice (TSF) Strombolian eruptive sequence. (b) Texturized Unmanned Aerial Vehicle (UAV) Photogrammetric 3D model of the uppermost excavation front showing the TSF Unit 2 with zoomed inset showing a ballistic lava block. (c) Oblique view of a texturized UAV Photogrammetric 3D model showing the preservation of the TSF pyroclastic units within a NW-SE trending graben. (d) Inset showing a normal fault displacing the base of the TSF Unit 1. Field picture of tilted, steeply dipping beds of the TSF Units 1 and 2, pervasively affected by faults. (f) Field picture of a structural contact between the TSF Unit 1 and the underlying paleosol. (g) Field picture of the TSF Unit 3 affected by conjugate faults producing metric displacements. (h) Zoomed field picture of a lava clast with a scoriaceous rim within TSF Unit 3. (i) Field picture showing a fault-controlled contact between the TSF Unit 2 and the underlying paleosol. (j) Zoomed photographs of a carbonate block embedded in the TSF Unit 2. (k) Field picture of an apophysis intruded within the paleosol succession. Outcrop locations are given in Figure 2a. Enlarged inset photographs are presented in Supporting Information S1.

10.1029/2023GC010994

Figure 5. (a) Texturized Unmanned Aerial Vehicle Photogrammetric 3D model oblique view of the eastern part of the quarry. (b) Field picture of the welded-spatter ramparts. (c) Detail of a welded-spatter rampart. (d and e) Close-up view of the welded scoriaceous lapilli and spatter deposits. (f and g) Field pictures of the lava flow deposit, showing both shear foliation and degassing structures, respectively. (h and i) Field photograph of the lava flow fronts at the base of the slope. Outcrop locations are given in Figures 2a and 5a. Enlarged inset photographs are presented in Supporting Information S1.

10.1029/2023GC010994

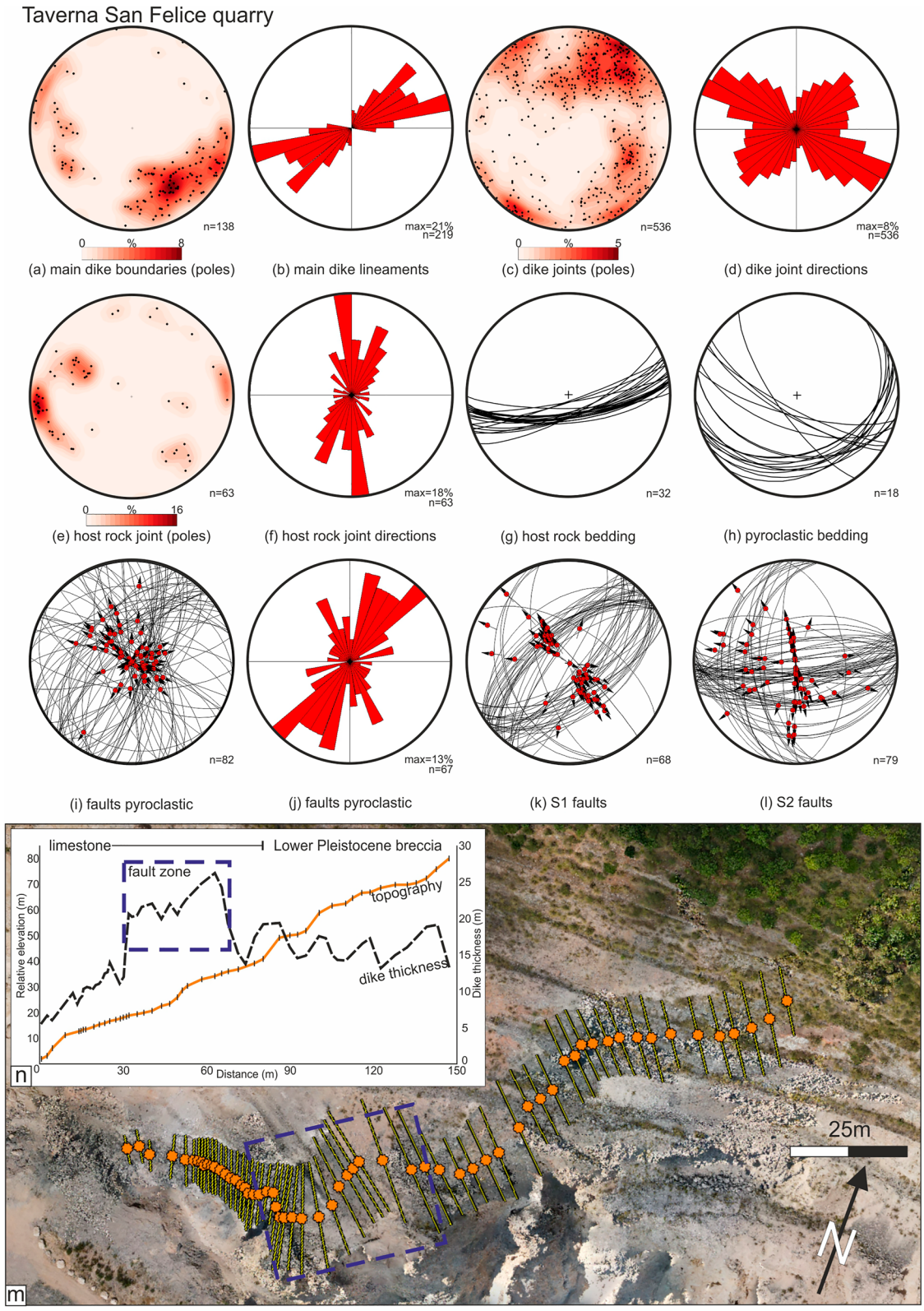

Figure 6.

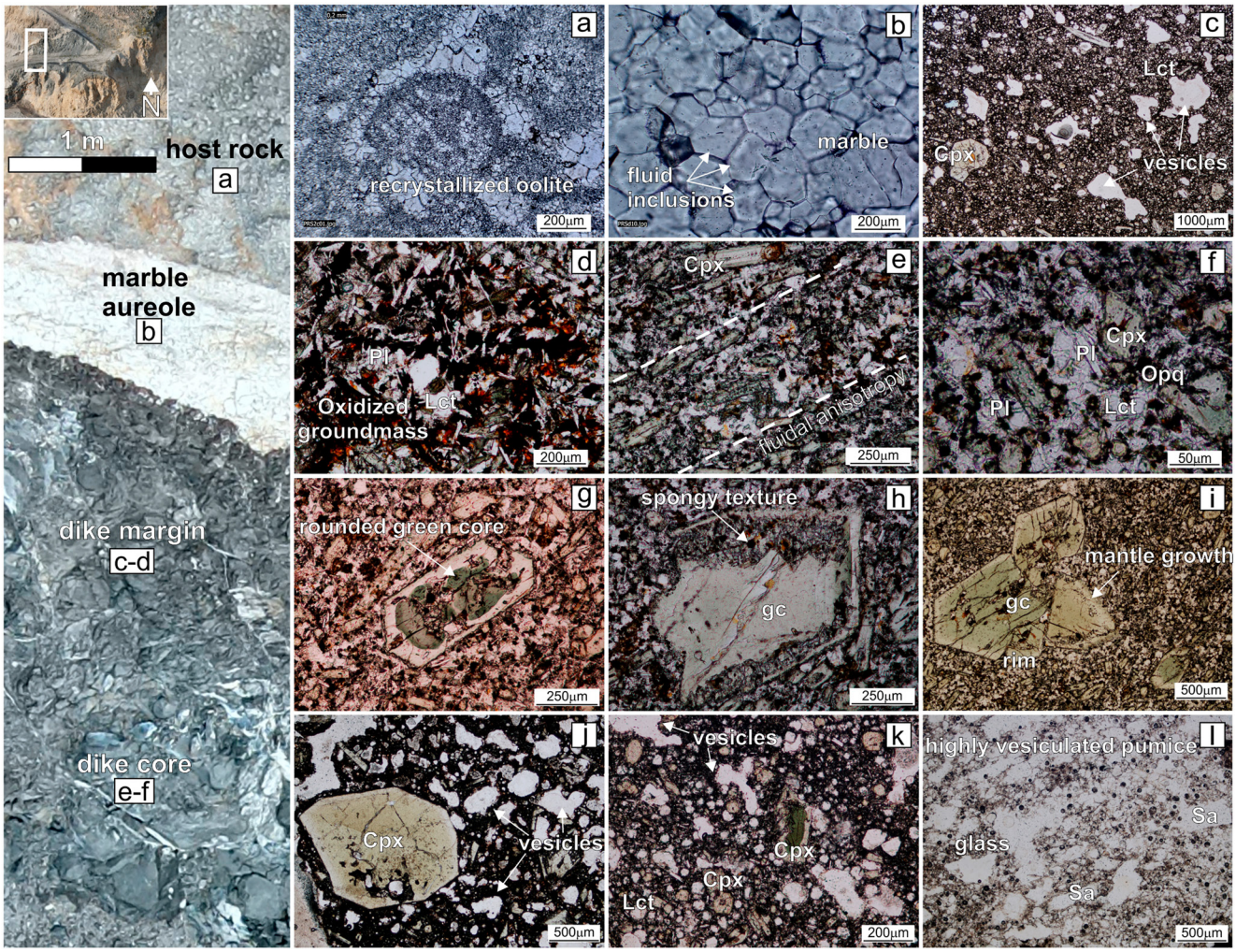

Figure 7. Left outcrop Unmanned Aerial Vehicle photograph shows the location of samples for panels (a–f), reporting representative plane polarized light photomicrographs of the investigated samples from the Taverna San Felice quarry. (a) Partially recrystallized limestone host rock with oolites; (b) Marble from the contact aureole; (c) Vesicle-rich dike margin with Cpx phenocrysts and Lct in the groundmass; (d) Oxidized groundmass on the dike margin; (e) Fluidal anisotropy defined by aligned Cpx microlites in dike core groundmass; (f) Dike core texture with Cpx, Pl and Lct microcrysts; (g) Cpx phenocryst with rounded green core; (h) green-core (gc) Cpx phenocryst with spongy texture; (i) green core Cpx phenocryst with mantle growth; Panels (j–l) show the petrography of the analyzed scoria, bomb and pumice clasts: (j) Weakly porphyritic, highly vesiculated scoria clast with zoned Cpx phenocryst; (k) weakly porphyritic and moderately vesiculated bomb clast with Cpx microphenocrysts and leucite (Lct) microlites; (l) highly vesiculated—poorly porphyritic pumice clast with rare sanidine (Sa) phenocrysts.

Roccamonfina. In the context of strong tectonic extension, the magma accumulated within crustal reservoirs (Figure 9a) can be forced to erupt since the negative buoyancy alone would not promote adiabatic magma uprise throughout the carbonate country rocks. Similar processes of magma intrusion beneath mountain ranges have been proposed for the nearby Matese ridge (Di Luccio et al., 2018) and reported for the central Apennines (Cardello et al., 2021).

The structural data and volcanological observations suggest that the morphostructural configuration at the time of the eruption was radically different from the present, highlighting that significant tectonic uplift took place after

Figure 6. Stereographic projections of poles to lineaments, joints, faults and bedding surface (lower hemisphere, equiareal net), with corresponding contour plots, rose diagrams and great circles. (a and b) Contour plot and rose diagram of main dike lineaments and measured contacts with the host rock. (c and d) Contour plot and rose diagram of dike joints. (e and f) Contour plot and rose diagram of host rock joints. (g) Great circle plot of bedding attitude of the carbonate host rock. (h) Great circle plot of bedding attitude of Taverna San Felice (TSF) pyroclastic deposit. (i) Great circle and slip vector of faults in the TSF pyroclastic deposits. (j) Rose diagram of the fault directions. (k) Great circle and slip vector of the S1 fault system measured in the host rock. (l) Great circle and slip vector of the S2 fault system measured in the host rock. (m) Orthomosaic nadiral view of TSF dike with measurement transects (orange lines) and midpoints (orange circles). The Blue dashed box indicates the approximate location of the main fault zone. (n) Plot of midpoint topography relative to the base of the quarry (orange line; the black ticks are the measuring points) and corresponding dike thickness (dashed black line). Horizontal distance is calculated across the midpoints.

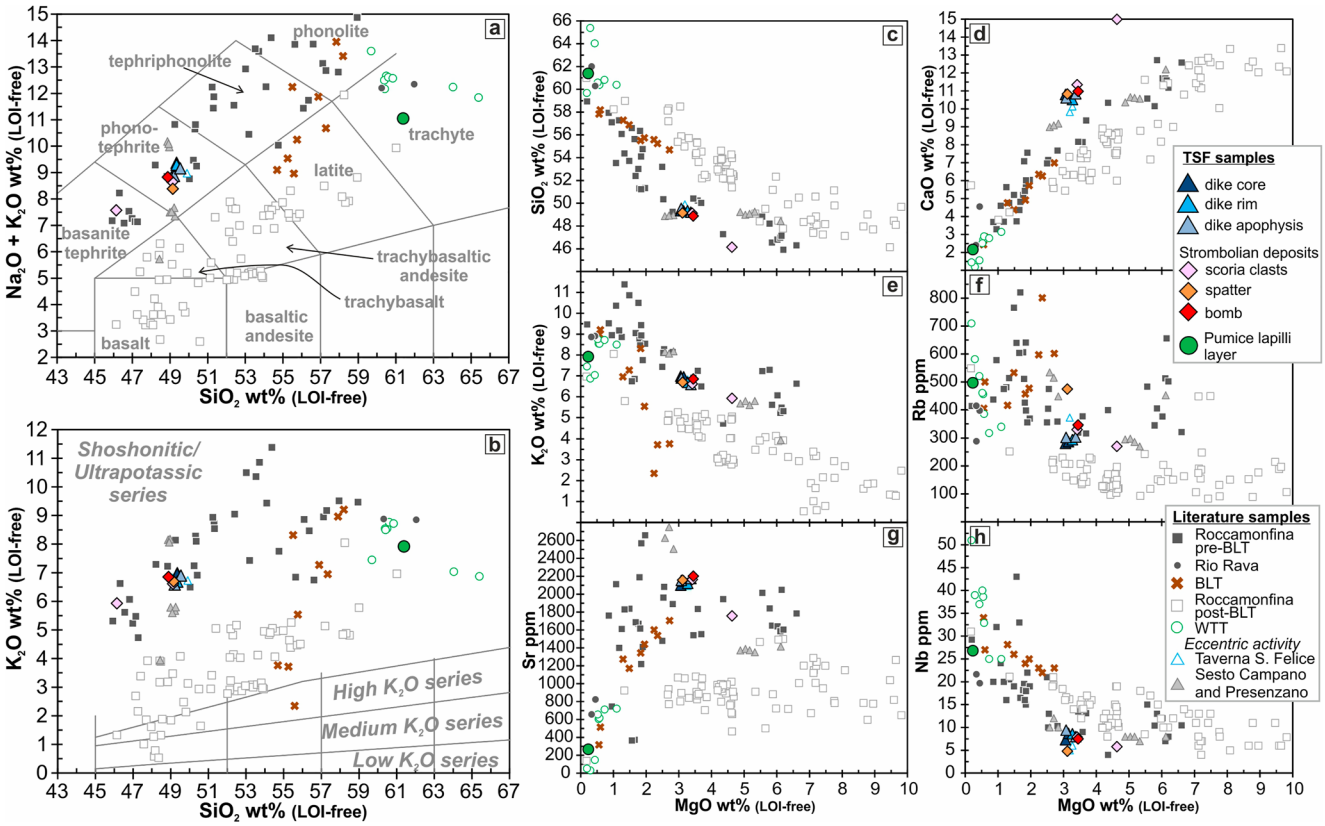

Figure 8. (a and b) Total Alkali versus Silica (TAS; Le Bas et al., 1986) and K_2O versus SiO_2 (Le Maitre et al., 2002), and (c–h) selected major oxides and trace elements versus MgO diagrams for the investigated samples from the Taverna San Felice (TSF) magmatic dike (dike core, dike margin, apophysis) and TSF Strombolian deposits and pumice lapilli layer. Literature samples for the Roccamonfina volcano (Beccaluva et al., 1991; Carter et al., 1978; Conticelli et al., 2002, 2007, 2009; D'Antonio et al., 1996; Di Girolamo, 1968; Giannetti, 1996, 2002; Giannetti & Ellam, 1994; Giannetti & Luhr, 1983; Hawkesworth & Vollmer, 1979; Luhr & Giannetti, 1987; Martelli et al., 2004; Rouchon et al., 2008; Santello, 2010; Vollmer, 1976; Vollmer & Hawkesworth, 1980), and for the peripheral vents of TSF, Sesto Campano and Presenzano, to the NE of the volcano edifice (Di Girolamo et al., 1991) are also reported for comparison.

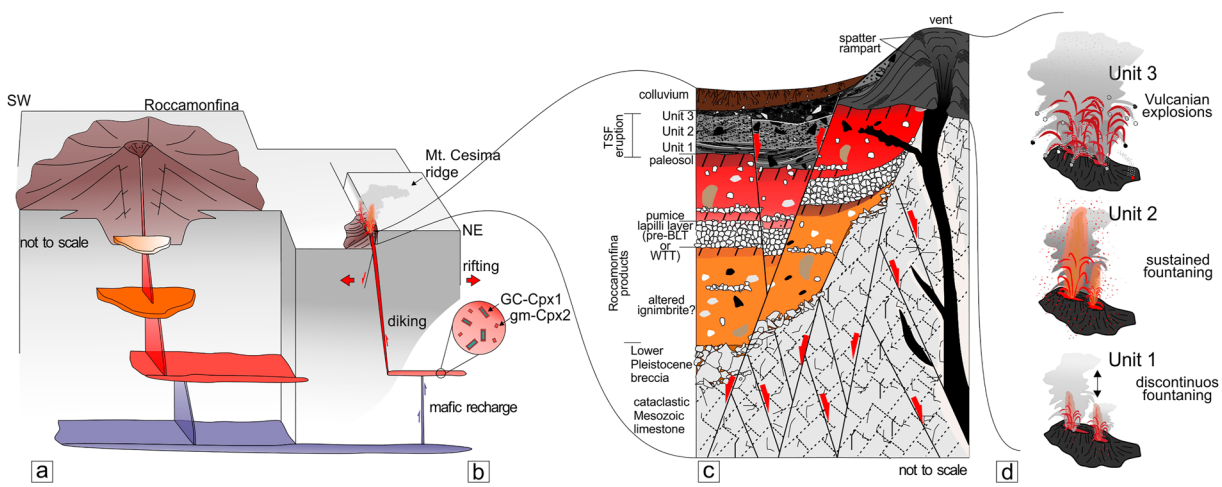

Figure 9. (a) Schematic cartoon showing a simplified model for the plumbing system beneath the Roccamonfina area. (b) Cartoon of the mafic recharge prior to the Taverna San Felice (TSF) eruption, according to the petrologic information. GC: Green Cores Cpx1 with more mafic mantle rim, and gm: groundmass Cpx2. (c) Simplified stratigraphic section showing the stratigraphic relationships between TSF products and Roccamonfina products. (d) Interpretative sketch illustrating the eruption processes emplacing the three units of the TSF Strombolian sequence.

the fissure eruption. In fact, carbonate clasts rarely occur in the thick paleosols underlying the TSF Strombolian deposits, indirectly suggesting the absence of significant eroding carbonate relief. However, more robust evidence is given by the presence of solidified magma within the uppermost portion of the dike exposure, where ramparts of welded spatter clasts were observed. Indeed, magmatic dikes resemble natural examples of hydraulic fracture fillings, and as such, they follow Pascal's Law of fluids. In case of pressure waning during the final stages of the eruption, the uppermost part of the dike would be drained following the drop in the magmastatic pressure. Therefore, since the fracture is filled by quenched magma up to its top, it indicates that the eruption was fed from a similar topographic level along the fissure length, with the magma solidifying at the sub-vent elevation as soon as the feeding was interrupted. The spatter ramparts constituting the vent system are found ∼160 m above the current plain level, which suggests that a corresponding uplift should have occurred at least since the end of the eruption. Therefore, depending on the stratigraphic attribution of this eruption (see following section), the uplift history of the Cesima ridge has occurred during or after the caldera phase of the Roccamonfina volcano.

5.2. Interpretation of Petrological Data

The composition of the TSF dike and Strombolian eruptive units is overall homogeneous and weakly evolved (tephritic to phonotephritic), indicating that the feeding magma had likely experienced limited differentiation before being erupted, in resemblance to the similar behavior of other carbonate-hosted monogenetic centers (e.g., Volsci Volcanic Field, Marra et al., 2021). Fractional crystallization is likely the main process involved, as indicated by the linear differentiation trends observed for most major oxides and trace elements (Figure 6 and Figures S1 and S2 in Supporting Information S1). These fall well within the larger differentiation trends defined by the pre-BLT Roccamonfina products, suggesting that the parental magmas from which the magmas generating the TSF volcanic rocks were likely similar to the least-evolved, near-primitive leucite-bearing basanitic magmas of the ancient volcano activity (Conticelli et al., 2009), which suggested Di Girolamo et al. (1991) to a straightforward correlation of this activity to this older phase. Nevertheless, the investigated samples display disequilibrium textures (i.a., green-cores Cpx, and growth mantle) typical of open-system processes such as magma mixing and/or contamination (Streck, 2008). The concentric reverse zoning in Cpx1 crystals can be interpreted as evidence of growth from a surrounding mafic liquid after the initial crystallization from a more evolved melt (Figure 9b). The rounded green cores with dissolved to spongy margins can represent the remnants of a magma batch before the homogenization with a more mafic recharge (Figure 9b). Significant mass change due to country-rock assimilation (e.g., Lucci et al., 2020) can be substantially excluded. The subordinate role of the open-system process is also testified by the very limited evidence for the ingestion of lithic clasts, which can be observed only in the outermost portions of the dike, close to the contact with the host rock. On the other hand, the presence of carbonate-bearing matrix embedding scoria clasts can be interpreted as a localized, short-lived hydromagmatic process due to magma intrusion in carbonate water-rich host rocks (Knuever et al., 2023).

Interestingly, the geochemical affinity of the TSF products is in line with that of the Roccamonfina pre-BLT products, belonging to the first period (630–400 ka) of strongly silica-undersaturated activity of the volcano. This is apparently in contrast with their stratigraphic position above the trachytic TSF pumice lapilli layer deposits that could be correlated with the WTT eruptions based on the juvenile compositions. Volcanological observations possibly support attribution to the latest of the WTTs unit, such as the Galluccio tuff ignimbrite (e.g., Giordano, 1998), which have at least two Plinian fallout deposits interstratified within the PDC deposits, dispersed toward the northeastern sector of the volcano. This would require some re-evaluation of the current petrological models for the magmatism in the Roccamonfina area, possibly indicating that the mantle sources responsible for the generation of strongly silica-undersaturated magmas, which dominated the oldest stages of activity (Conticelli et al., 2009; see Section 2), could have been reactivated in more recent times in the peripheral sectors of the volcano.

5.3. Stratigraphy of TSF Strombolian Eruption

The TSF Strombolian pyroclastic sequence shows a regular basal contact on the underlying paleosol, which embeds a pumice lapilli layer (Figure 9c). As concerns the TSF dike, it reached the surface and fed a fissure eruption which emplaced three eruptive units characterized by vesiculated scoria clasts and frequent carbonate and lava clasts as lithic ballistics. These three units have been distinguished based on deposit lithofacies and changes in grain size. We reconstructed the eruptive sequence as follows: Unit 1 is the result of discontinuous

lava fountaining, with the ejection of pyroclasts producing a stratified deposit, featuring frequent scoriaceous spatter clasts and carbonate bombs (Figure 9d). The presence of whitish fine-grained scoria lapilli layers possibly witnesses some short-lived phases of carbonate-rich water-magma interaction during eruption column pulsation. Unit 2 is characterized by a coarser and massive deposit, mainly composed of spatter clasts and bombs with ballistic carbonate blocks, interpreted as a peak of the sustained fountaining phase of the eruption with clast agglutination might suggesting a relatively higher emplacement temperature (Figure 9d). Episodic water-magma interactions are suggested by carbonate-coated finer lapilli beds. Unit 3 indicates episodic, more energetic explosions (i.e., Vulcanian, Figure 9d) involving already solidified portions of the dike, as suggested by the presence of frequent, up to meter-sized, solidified lava clasts embedded into poorly vesiculated scoria material (e.g., Figure 4h). The reddish color of this Unit suggests enhanced oxidation due to high emplacement temperature. The topmost contact is poorly preserved, but locally the sequence is covered by colluvium and slope talus deposits, which rework the pyroclastic material. In summary, the stratigraphic data suggest the occurrence of a Strombolian/fissure eruption, characterized by low-to-moderate energy lava fountaining, possibly from a series of vents that are only locally preserved.

5.4. The "Thickness Problem" and Estimate of the Magma Overpressure

The reconstruction of the dike geometry based on structural and field data indicates an average thickness of 5 m in the lower part and >25 m in some segments of the middle part, with an average thickness of ~20 m (Figures 6m and 6n). Compared to other examples of magmatic dikes worldwide, from the Italian volcanoes of Etna (1.9 m, Scudero et al., 2019) and Somma-Vesuvius (1.2 m, Porreca et al., 2006), the Mijakejima island (Japan, 1.3 m, Geshi & Oikawa, 2014), the Icelandic East Rift zone (4 m, Gudmundsson, 1983) and Askja volcano (0.8 m, Trippanera et al., 2018), the Oslo Rift (Norway, <2 m, Poppe et al., 2020), the Timna Igneous Complex (Israel, 1.5–32 m, Baer et al., 1994), and the Santorini island (Greece, 2–10 m, Drymoni et al., 2022), the thickness of TSF dike is well above the average. The only comparable cases are those from the East Rift and Timna Igneous Complex, which however exceed 3 and 1 km in length, respectively, whereas the exposed TSF dike is less than 1 km. Furthermore, a thickness >20 m would require significant magma overpressure (Geshi et al., 2020), but volcanological and petrographic observations suggest that the magma was only moderately vesiculated, both in the solidified lava and the ballistic juvenile material, likely indicating low magma overpressure, following the relationship proposed by Geshi et al. (2020).

On the other hand, the absence of diagnostic structures, such as multiple joint rows or internal chilled margins, indicates that such large thickness could not result from multiple magma injections (sensu Gudmundsson, 1984). Therefore, we propose that the unusually large thickness of the TSF dike is related to a spectrum of factors that include the lack of constraints at the free surface (Geshi et al., 2010, 2020), the effect of dilatant component of normal faults during rifting (Weismuller et al., 2019), and the pre-existing very-low rigidity damage zone of NE-SW faults, that magma re-used in localized oblique opening during propagation, as suggested by the deviation from E-W to NE-SW orientation, and already observed in monitored rifting events (Ruch et al., 2016).

Another concurrent factor might be found in dike-wall erosion processes during magma ascent within the host rock (Geshi & Oikawa, 2014), although is less common in mild-Strombolian eruptions (e.g., Morgan et al., 2008), and not envisaged by the few amounts of carbonate lithic clasts found within the dike.

The geometry of a magmatic dike may give clues on the overpressure needed to break the magma reservoir and reach the surface. A representative dike thickness (w) of 5 m, has been measured in the lowermost part of the quarry. According to the distribution of welded deposits and direct outcrop measurements, the strike-dimension (L) of the dike is inferred to be 1,000 m, resulting in an aspect ratio L/w of 200, within the literature-estimated ranges of 10^2–10^3 (Gudmundsson, 1983). The relationship between the overpressure of magma filling a dike in an elastic medium (P_o) and the dike aspect ratio L/w in a two-dimensional elliptical crack is defined as follows:

$$P_O = \frac{wE}{2L(1-v^2)} \quad (1)$$

where E is the Young's modulus and v is the Poisson's ratio (Gudmundsson, 2020; Pollard & Segall, 1987). Assuming E equal to 10^{10} Pa and v 0.25, Po is ~26×10^6 Pa.

However, for a dike that leaves the magma reservoir and propagates into the upper crust, the magmatic overpressure is also defined as follows:

$$P_O = P_e + (\rho_r - \rho_m)gh + \sigma_d \quad (2)$$

where P_e is the magmatic excess pressure, which is equal to the in situ tensile strength of the host rock. The buoyancy term is a function of the density difference between the host rock ρ_r and the magma ρ_m, multiplied by gravity acceleration g and depth h. The tectonic differential stress σ_d is defined as $\sigma_d = \sigma_1 - \sigma_3$ in the considered crustal layers. Magmatic excess pressure *Pe* usually ranges between 3 and 10×10^6 Pa (Gudmundsson, 2012), assuming an average ρ_r of 2,400 kg m^{-3} for the limestones and basement rocks and ρ_m of 2,650 kg m^{-3} for a basanite/tephrite magma, with g 9.81 m s^{-2}, and h given by the dip-dimension of the dike, (i.e., the depth of the magma chamber) at 10^4 m. Therefore, the buoyancy term is negative at ca. -24×10^6 Pa, thus strongly hampering magmatic overpressure P_o. Many observations indicate that tectonic differential stress σ_d may be the main factor controlling the dike intrusion, ranging between 40 and 47×10^6 Pa (remarkably similar to σ_d values necessary to produce normal faulting in extensional settings, e.g., Fossen, 2016), implying that the P_e alone would not be sufficient to drive the eruption. In fact, the low viscosity of the magma that can be inferred based on the geometry of the tips (e.g., wedge-like) and the moderately/low vesicularity is in contrast with the significant thickness of the dike. Indeed, following Geshi et al. (2020), the dike aspect ratio may help distinguish between magmas of high and low vesicularity, thus resulting in corresponding explosivity eruptions. Higher vesicularity was only observed in the main dike along the contact with the host rock and around carbonate enclaves. Hence, low confining pressure due to tectonic extension is likely the main factor controlling the "passive" dike intrusion (sensu Cervelli et al., 2002).

5.5. Outcrop-Scale Magma Intrusion Mechanism

Regarding the intrusion mechanism of the TSF dike, two possible processes could be suggested. Pure-opening deformation (Mode I) seems to be dominant in the bottom part of the exposed dike, where the host rock is made by the Lower Cretaceous limestones (Figure 1c), as testified by the sharp contacts and wedge-like tapered tips (Figure 3). Moreover, the observed peperite-like dikes (Figure 3j) may be interpreted as preserved fluid-filled cavity tips of propagating apophysis (Poppe et al., 2020 and references therein) where localized magma-water interactions occurred (Westerman et al., 2017). Blunt geometries of some tips, irregular contacts, the larger thickness of the dike toward the tips, as well as plastic deformation of the low-rigidity material indicate a shear-dominated deformation (Mode II), as similarly observed in the literature (Dering et al., 2019; Martinez-Poza & Druguet, 2016). This is the case where the host rock consists of cataclastic limestones, like in the uppermost part of the outcrop (Figure 4). Thus, we hypothesize that the low-confining pressure related to near-surface dilatant fractures, the deterioration of the host rock due to cataclasis, and the thermo-chemical interaction (e.g., decarbonation and dissolution) concurrently played a role in the dike intrusion. Similar processes are envisaged also in the Volsci Volcanic Field (Marra et al., 2021). In particular, the effect of a pre-existing fault zone in near-surface conditions likely affected dike propagation, as hinted by the field evidence that the direction of the dike deviated from E-W to NE-SW, since σ_n to the fault plane is lower than σ_3 (e.g., Gudmundsson, 2011). In a general perspective, this highlights the pivotal role that volcano-tectonic setting, such as fault-related fracture zones, may have during magma propagation, with potential repercussions on vent location (e.g., González, 2022). Finally, it seems likely that the intrusion of the dike was accompanied by the pervasive circulation of CO_2-rich fluids, as evidenced by the pseudo-karst features observed both in the TSF quarry and in the nearby areas. Indeed, heating of the host rock could have promoted carbonate dissolution in circulating waters, followed by calcite re-precipitation in open fractures and porosities, similar to intrusion-related geothermal systems (Stimac et al., 2015).

5.6. Evolutionary Model

In Figure 10, we summarize the volcano-tectonic evolutionary stages that can be inferred for the TSF dike intrusion, starting from a flatter initial morphology (Figure 10a) in which only a small relief is present above a NE-SW and NW-SE oriented flank, the latter not represented in the figure. NE-SW faults affect the entire Mt Cesima succession, including Mesozoic carbonates and Lower Pleistocene breccia, and are formerly covered by altered Roccamonfina ignimbrite and fallout deposits. The dike intrusion started during an N-S extensional pulse (Figure 10a), promoting magma chamber rupture and magma propagation from beneath the former plain. The main intrusion mechanism is a pure-opening mode I (Figure 10b). As magma reaches the surface along a E-W oriented permeable fractures, with sub-surficial mixed-mode intrusion mechanism (Figure 10c), and several smaller apophyses. With the onset of the eruption, the aquifer circulation is altered as denoted by thermal springs (Figure 10c) witnessed by the speleothem features. The along-strike propagation of the dike intercepted the pre-existing NE-SW oriented fault zone (Figure 10d), whose greater permeability promoted lateral propagation

10.1029/2023GC010994

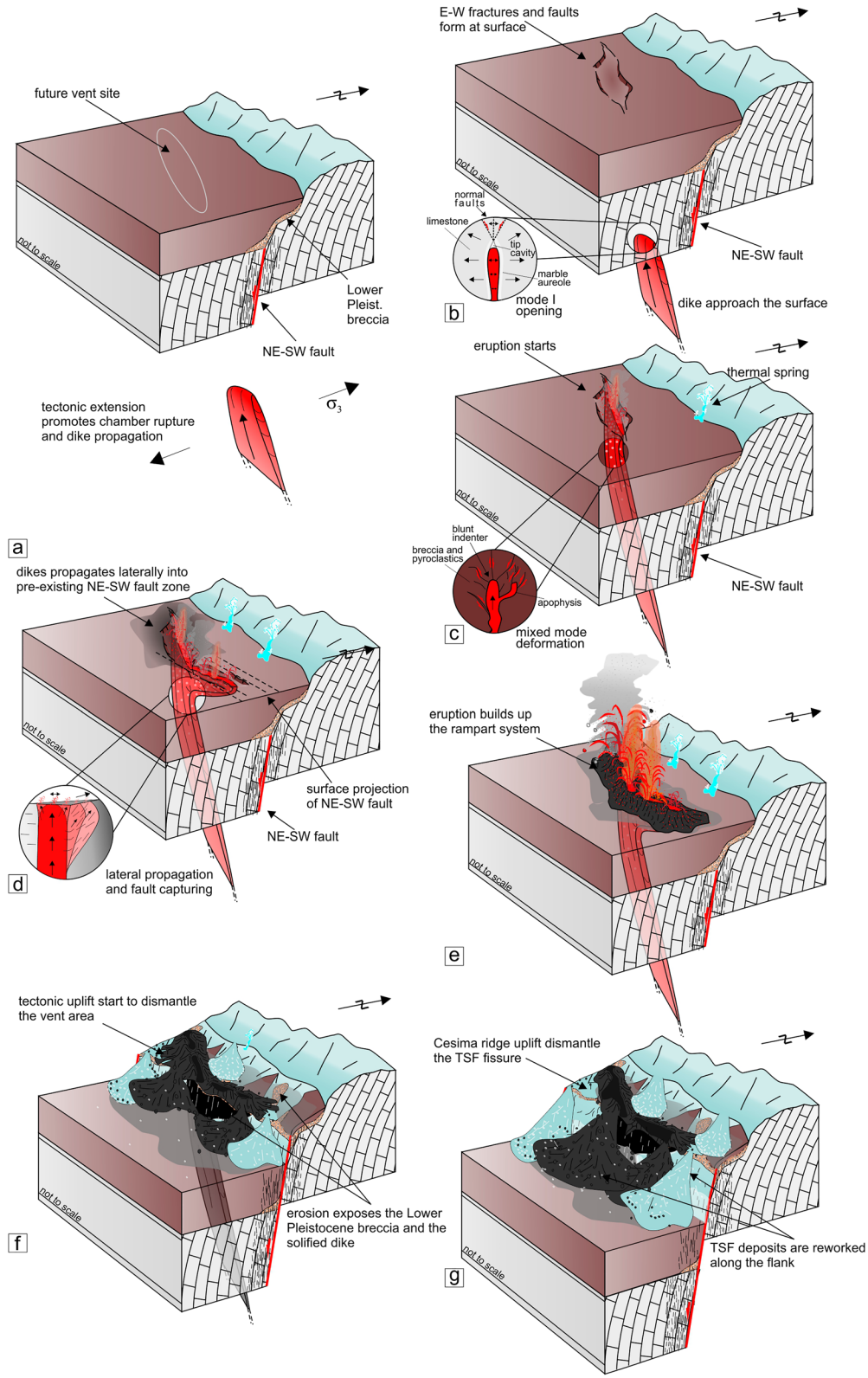

Figure 10. Cartoon showing the proposed volcano-tectonic evolution of the southern sector of Mt Cesima ridge. See the text for full explanations.

and dike thickening. As the eruption continued, a compound spatter rampart system built up (Figure 10e), concurrently with the emission of pyroclasts and subordinate lava flows. Following the eruption, potentially concurrently with the caldera period of Roccamonfina, the uplift of the Mt. Cesima ridge started to dismantle the vent (Figure 10f), and locally exposed underlying deposits. In the final stage of the model, the uplift of the Mt. Cesima ridge had elevated the spatter system midway along the flank, as well as the Lower Pleistocene breccia, found at higher elevations (Figure 10g). Reworked deposits develop a less-steep flank.

6. Conclusions

In this work, we studied one of the most impressive outcrops of a magmatic dike intruded within carbonates in central-southern Italy, merging structural, stratigraphic, and petrological analyses. The tephritic TSF dike, broadly E-W oriented, was intruded within the southern edge of the Mt Cesima ridge, northeast of the Roccamonfina volcano. The dike intrusion was promoted by an important extensional event during the Middle Pleistocene that affected the Tyrrhenian margin of the southern Apennines and could be either younger than pre-BLT eruptions (~440 ka) or of the WTT Plinian eruptions (310–230 ka) of Roccamonfina volcano. The dike fed an eruption over a ~1 km long fissure, which emplaced a composite pyroclastic eruptive sequence up to 10 m thick. The combination of near-surface dilatant cracks and the intersection of preexisting fault damage zones account for the large thickness of the dike. Furthermore, the structural position of these volcanics suggests that they are closely related to the Mt. Cesima uplift, since these vent structures and the Lower Pleistocene breccia are currently found at over 160 m above the plain level, indicating that the whole ridge has undergone significant uplift after the dike intrusion episode.

Our data suggest that the eruption of the TSF dike and associated pyroclastics were sourced by a magma reservoir uncorrelated to that of the Roccamonfina volcano, highlighting the leading role of the extensional tectonics in this area during the Middle Pleistocene. Further analysis, including new geochronological data, is necessary to provide an unambiguous temporal framework for the eruption, which could be presently ascribed to both the pre-caldera and the post-caldera periods of Roccamonfina activity. The occurrence of a peripheral feeder dike and its subsequent exhumation and uplift suggests regional-scale extensional events that controlled the localization of volcanism in this area of the Tyrrhenian margin of the southern Apennines. A similar mechanism could be possibly depicted also for the onset of volcanism in the Campania Plain, where the Campi Flegrei caldera, Ischia and Somma-Vesuvius developed. Detailed structural data also point out that dike propagation can be strongly influenced by fault fracture networks that can alter the trajectory beyond the control of local stress fields.

Acknowledgments
This work was supported by the University of Naples Federico II in the framework of Jacopo Natale's PhD project. This article is based on the last chapter of his doctoral dissertation. This work received no specific grants or funds from public or private institutions. The Authors are grateful to Colacem SPA for granting the access to the quarry and furnishing the needed support to perform the geological surveys. Dr. Rita Mele of Regione Campania is acknowledged for her availability and cooperation. Dr. Gerardo Iacovone is acknowledged for his cooperation and support. The operators of the quarry are kindly acknowledged for their help. JN is profoundly grateful to Mario Scardino for his invaluable support, kindness, and cooperation during the uncountable field campaigns. This work benefitted from a useful discussion with Paola Petrosino. Luca Giovanni Cardello and an anonymous Reviewer are acknowledged for their constructive comments that improved the manuscript. JN acknowledges Dr. Pasquale Allocca for his help in the field. The University of Bari Aldo Moro is acknowledged for covering the Article Publication Charges (APCs) within the CARE Agreement.

Conflict of Interest

The authors declare no conflicts of interest relevant to this study.

Data Availability Statement

Data are available at Natale (2023).

References

Alessandri, L., Cardello, G. L., Attema, P. A. J., Baiocchi, V., De Angelis, F., Del Pizzo, S., et al. (2021). Reconstructing the Late Pleistocene–Anthropocene interaction between the neotectonic and archaeological landscape evolution in the Apennines (La Sassa cave, Italy). *Quaternary Science Reviews*, *265*, 107067. https://doi.org/10.1016/j.quascirev.2021.107067

Amato, V., Aucelli, P. P., Cesarano, M., Jicha, B., Lebreton, V., Orain, R., et al. (2014). Quaternary evolution of the largest intermontane basin of the Molise Apennine (central-southern Italy). *Rendiconti Lincei*, *25*(S2), 197–216. https://doi.org/10.1007/s12210-014-0324-y

Appleton, J. D. (1972). Petrogenesis of potassium-rich lavas from the Roccamonfina volcano, Roman Region, Italy. *Journal of Petrology*, *13*(3), 425–456. https://doi.org/10.1093/petrology/13.3.425

Baer, G., Beyth, M., & Reches, Z. E. (1994). Dikes emplaced into fractured basement, Timna igneous complex, Israel. *Journal of Geophysical Research*, *99*(B12), 24039–24050. https://doi.org/10.1029/94jb02161

Ballini, A., Barberi, F., Laurenzi, M. A., Mezzetti, F., & Villa, I. M. (1989). Nuovi dati sulla stratigrafia del vulcano di Roccamonfina. *Bollettino Gruppo Nazionale Vulcanologia*, *5*(2), 533–555.

Beccaluva, L., Di Girolamo, P., & Serri, G. (1991). Petrogenesis and tectonic setting of the Roman Volcanic Province, Italy. *Lithos*, *26*(3–4), 191–221. https://doi.org/10.1016/0024-4937(91)90029-k

Bergomi, C., Catenacci, V., Cestari, G., Manfredini, M., & Manganelli, V. (1969). *Note illustrative della Carta Geologica d'Italia F. 171 Gaeta e Vulcano di Roccamonfina*. Servizio Geologico d'Italia.

Boncio, P., Dichiarante, A. M., Auciello, E., Saroli, M., & Stoppa, F. (2016). Normal faulting along the western side of the Matese Mountains: Implications for active tectonics in the Central Apennines (Italy). *Journal of Structural Geology*, *82*, 16–36. https://doi.org/10.1016/j.jsg.2015.10.005

Bosi, V. (1994). Evoluzione neotettonica del Lazio Meridionale Campania Settentrionale, in corrispondenza della terminazione meridionale della linea tettonica «Ortona-Roccamonfina. Doctoral dissertation. Tesi di Dottorato di Ricerca, VI ciclo. Dipartimento di Scienze della Terra. Università «La Sapienza».

Bosi, V., & Giordano, G. (1997). Stress field evolution in central Italy during middle-late Pleistocene: New information from southern Latium. *Il Quaternario*, *10*(2), 631–636.

Buono, G., Pappalardo, L., Harris, C., Edwards, B. R., & Petrosino, P. (2020). Magmatic stoping during the caldera-forming Pomici di Base eruption (Somma-Vesuvius, Italy) as a fuel of eruption explosivity. *Lithos*, *370*, 105628. https://doi.org/10.1016/j.lithos.2020.105628

Caiazzo, C., Ascione, A., & Cinque, A. (2006). Late Tertiary–Quaternary tectonics of the Southern Apennines (Italy): New evidences from the Tyrrhenian slope. *Tectonophysics*, *421*(1–2), 23–51. https://doi.org/10.1016/j.tecto.2006.04.011

Cardello, G. L., Consorti, L., Palladino, D. M., Carminati, E., Carlini, M., & Doglioni, C. (2020). Tectonically controlled carbonate-seated maar-diatreme volcanoes: The case of the Volsci Volcanic Field, central Italy. *Journal of Geodynamics*, *139*, 101763. https://doi.org/10.1016/j.jog.2020.101763

Cardello, G. L., Vico, G., Consorti, L., Sabbatino, M., Carminati, E., & Doglioni, C. (2021). Constraining the passive to active margin tectonics of the internal central Apennines: Insights from biostratigraphy, structural, and seismic analysis. *Geosciences*, *11*(4), 160. https://doi.org/10.3390/geosciences11040160

Carminati, E., Fabbi, S., & Santantonio, M. (2014). Slab bending, syn-subduction normal faulting, and out-of-sequence thrusting in the Central Apennines. *Tectonics*, *33*(4), 530–551. https://doi.org/10.1002/2013tc003386

Carter, S. R., Evensen, N. M., Hamilton, P. J., & O'nions, R. K. (1978). Continental volcanics derived from enriched and depleted source regions: Nd-and Sr-isotope evidence. *Earth and Planetary Science Letters*, *37*(3), 401–408. https://doi.org/10.1016/0012-821x(78)90055-9

Cervelli, P., Segall, P., Amelung, F., Garbeil, H., Meertens, C., Owen, S., et al. (2002). The 12 September 1999 upper east rift zone dike intrusion at Kilauea volcano, Hawaii. *Journal of Geophysical Research*, *107*(B7), ECV–3. https://doi.org/10.1029/2001jb000602

Ciaranfi, N., Guida, M., Iaccarino, G., Pescatore, T., Pieri, P., Rapisardi, L., et al. (1983). Elementi sismotettonici dell'Appennino meridionale. *Bollettino della Societa Geologica Italiana*, *102*(2–3), 201–222.

Cinque, A., Ascione, A., & Caiazzo, C. (2000). *Distribuzione spazio-temporale e caratterizzazione della fagliazione quaternaria in Appennino meridionale* (pp. 203–218). Le ricerche del GNDT nel campo della pericolosità sismica.

Cole, P. D., Guest, J. E., & Duncan, A. M. (1993). The emplacement of intermediate volume ignimbrites: A case study from Roccamonfina Volcano, Southern Italy. *Bulletin of Volcanology*, *55*(7), 467–480. https://doi.org/10.1007/bf00304590

Cole, P. D., Guest, J. E., Duncan, A. M., Chester, D. K., & Bianchi, R. (1992). Post-collapse volcanic history of calderas on a composite volcano: An example from Roccamonfina, southern Italy. *Bulletin of Volcanology*, *54*(4), 253–266. https://doi.org/10.1007/bf00301481

Conte, A. M., Perinelli, C., Bosman, A., Castorina, F., Conti, A., Cuffaro, M., et al. (2020). Tectonics, dynamics, and Plio-Pleistocene magmatism in the Central Tyrrhenian Sea: Insights from the submarine transitional basalts of the Ventotene Volcanic Ridge (Pontine Islands, Italy). *Geochemistry, Geophysics, Geosystems*, *21*(12), e2020GC009346. https://doi.org/10.1029/2020gc009346

Conticelli, S., Carlson, R. W., Widom, E., & Serri, G. (2007). Chemical and isotopic composition (Os, Pb, Nd, and Sr) of Neogene to Quaternary calc-alkalic, shoshonitic, and ultrapotassic mafic rocks from the Italian peninsula: Inferences on the nature of their mantle sources.

Conticelli, S., D'antonio, M., Pinarelli, L., & Civetta, L. (2002). Source contamination and mantle heterogeneity in the genesis of Italian potassic and ultrapotassic volcanic rocks: Sr–Nd–Pb isotope data from Roman Province and Southern Tuscany. *Mineralogy and Petrology*, *74*(2–4), 189–222. https://doi.org/10.1007/s007100200004

Conticelli, S., Laurenzi, M. A., Giordano, G., Mattei, M., Avanzinelli, R., Melluso, L., et al. (2010). Leucite-bearing (kamafugitic/leucititic) and-free (lamproitic) ultrapotassic rocks and associated shoshonites from Italy: Constraints on petrogenesis and geodynamics. *Journal of the Virtual Explorer*, *36*(20), 1–95. https://doi.org/10.3809/jvirtex.2010.00251

Conticelli, S., Marchionni, S., Rosa, D., Giordano, G., Boari, E., & Avanzinelli, R. (2009). Shoshonite and sub-alkaline magmas from an ultrapotassic volcano: Sr–Nd–Pb isotope data on the Roccamonfina volcanic rocks, Roman Magmatic Province, Southern Italy. *Contributions to Mineralogy and Petrology*, *157*(1), 41–63. https://doi.org/10.1007/s00410-008-0319-8

D'Agostino, N., Chamot-Rooke, N., Funiciello, R., Jolivet, L., & Speranza, F. (1998). The role of pre-existing thrust faults and topography on the styles of extension in the Gran Sasso range (central Italy). *Tectonophysics*, *292*(3–4), 229–254. https://doi.org/10.1016/s0040-1951(98)00070-5

D'Antonio, M., Tilton, G. R., & Civetta, L. (1996). Petrogenesis of Italian alkaline lavas deduced from Pb-SrNd isotope relationships. In A. BASU, & S. HART (Eds.), *Earth processes: Reading the isotopic code* (Vol. 95, pp. 253–267). AGU Monograph Series.

Demangeot, J. (1965). *Géomorphologie des Abruzzes adriatiques* (Vol. 1). Éditions du Centre national de la recherche scientifique.

De Matteo, A., Corti, G., de Vries, B. V. W., Massa, B., & Mussetti, G. (2018). Fault-volcano interactions with broadly distributed stretching in rifts. *Journal of Volcanology and Geothermal Research*, *362*, 64–75. https://doi.org/10.1016/j.jvolgeores.2018.08.008

Dering, G. M., Micklethwaite, S., Cruden, A. R., Barnes, S. J., & Fiorentini, M. L. (2019). Evidence for dyke-parallel shear during syn-intrusion fracturing. *Earth and Planetary Science Letters*, *507*, 119–130. https://doi.org/10.1016/j.epsl.2018.10.024

De Rita, D., & Giordano, G. (1996). Volcanological and structural evolution of Roccamonfina volcano (Italy): Origin of the summit caldera. *Geological Society, London, Special Publications*, *110*(1), 209–224. https://doi.org/10.1144/gsl.sp.1996.110.01.16

De Rita, D., Giordano, G., & Milli, S. (1998). Forestepping-backstepping stacking pattern of volcaniclastic successions: Roccamonfina volcano, Italy. *Journal of Volcanology and Geothermal Research*, *80*(1–2), 155–178. https://doi.org/10.1016/s0377-0273(97)00069-3

Di Girolamo, P. (1968). Rilevamento petrografico nel settore SW (Sessa Aurunca) del Vulcano di Roccamonfina. *Rendiconti Accademia Scienze Fisiche e Matematiche Naples*, *35*, 675–722.

Di Girolamo, P. (1972). II cono di scorie eccentrico di Sesto Campana (Isernia) (vulcano di Roccamonfina). *Bollettino della Societa dei Naturallsti in Napoli*, *81*, 31–50.

Di Girolamo, P., Melluso, L., & Morra, V. (1991). Magmatic activity northeast of Roccamonfina volcano (Southern Italy): Petrology, geochemistry and relationships with campanian volcanics. *Neues Jahrbuch für Mineralogie—Abhandlungen*, *163*, 271–289.

Di Girolamo, P., & Morra, V. (1988). Il magmatismo mesozoico-quaternario della Campania: Petrologia e significato geodinamico. *Memorie della Societa Geologica Italiana*, *41*, 165–179.

Di Girolamo, P., Morra, V., Ortolani, F., & Pagliuca, S. (1988). Segnalazione di lava basanitica leucitica nella Piana del Volturno. *Bollettino della Societa dei Naturalisti in Napoli*, *107*, 561–578.

Di Luccio, F., Chiodini, G., Caliro, S., Cardellini, C., Convertito, V., Pino, N. A., et al. (2018). Seismic signature of active intrusions in mountain chains. *Science Advances*, *4*(1), e1701825. https://doi.org/10.1126/sciadv.1701825

Drymoni, K., Browning, J., & Gudmundsson, A. (2022). Spatial and temporal volcanotectonic evolution of Santorini volcano, Greece. *Bulletin of Volcanology*, *84*(6), 60. https://doi.org/10.1007/s00445-022-01566-4

Faccenna, C., Davy, P., Brun, J. P., Funiciello, R., Giardini, D., Mattei, M., & Nalpas, T. (1996). The dynamics of back-arc extension: An experimental approach to the opening of the Tyrrhenian Sea. *Geophysical Journal International*, *126*(3), 781–795. https://doi.org/10.1111/j.1365-246x.1996.tb04702.x

Favela, J., Anderson, D. L., & Boschi, E. (2000). Extensional tectonics and global volcanism. *Problems in Geophysics for the new Millennium*, 463–498.

Fossen, H. (2016). *Structural geology*. Cambridge University Press.

Galderisi, A., Galli, P., Mazzoli, S., & Peronace, E. (2017). Kinematic constraints of the active northern Matese Fault System (southern Italy). *Bollettino di Geofisica Teorica ed Applicata*, *58*(4).

Galindo, I., & Gudmundsson, A. (2012). Basaltic feeder dykes in rift zones: Geometry, emplacement, and effusion rates. *Natural Hazards and Earth System Sciences*, *12*(12), 3683–3700. https://doi.org/10.5194/nhess-12-3683-2012

GeoVis3D software package. (2022). GeoVis3D software package. Retrieved from https://www.ausgeol.org\geovis3d

Geshi, N., Browning, J., & Kusumoto, S. (2020). Magmatic overpressures, volatile exsolution and potential explosivity of fissure eruptions inferred via dike aspect ratios. *Scientific Reports*, *10*(1), 1–9. https://doi.org/10.1038/s41598-020-66226-z

Geshi, N., Kusumoto, S., & Gudmundsson, A. (2010). Geometric difference between non-feeder and feeder dikes. *Geology*, *38*(3), 195–198. https://doi.org/10.1130/g30350.1

Geshi, N., & Oikawa, T. (2014). The spectrum of basaltic feeder systems from effusive lava eruption to explosive eruption at Miyakejima volcano, Japan. *Bulletin of Volcanology*, *76*(3), 1–14. https://doi.org/10.1007/s00445-014-0797-7

Giaccio, B., Hajdas, I., Isaia, R., Deino, A., & Nomade, S. (2017). High-precision ^{14}C and $^{40}Ar/^{39}Ar$ dating of the Campanian Ignimbrite (Y-5) reconciles the time-scales of climatic-cultural processes at 40 ka. *Scientific Reports*, *7*(1), 1–10. https://doi.org/10.1038/srep45940

Giannetti, B. (1990). Strutture neotettoniche presenti nel tufo trachitico bianco del vulcano di Roccamonfina. *Bollettino Servizio Geologico Italiano*, *109*, 195–206.

Giannetti, B. (1996). The geology of the yellow trachytic tuff, Roccamonfina volcano, Italy. *Journal of Volcanology and Geothermal Research*, *71*(1), 53–72. https://doi.org/10.1016/0377-0273(95)00030-5

Giannetti, B. (2002). Coarse-grained and porphyritic inclusions in phonolitic lavas, Roccamonfina volcano, Italy. *Journal of Volcanology and Geothermal Research*, *117*(3–4), 297–325. https://doi.org/10.1016/s0377-0273(02)00227-5

Giannetti, B., & Ellam, R. (1994). The primitive lavas of Roccamonfina volcano, Roman region, Italy: New constraints on melting processes and source mineralogy. *Contributions to Mineralogy and Petrology*, *116*(1–2), 21–31. https://doi.org/10.1007/bf00310687

Giannetti, B., & Luhr, J. F. (1983). The white trachytic tuff of Roccamonfina volcano (Roman region, Italy). *Contributions to Mineralogy and Petrology*, *84*(2–3), 235–252. https://doi.org/10.1007/bf00371289

Giordano, G. (1998). Facies characteristics and magma–water interaction of the White Trachytic Tuffs (Roccamonfina Volcano, southern Italy). *Bulletin of Volcanology*, *60*(1), 10–26. https://doi.org/10.1007/s004450050213

Giordano, G., Naso, G., Scrocca, D., Funiciello, R., & Catalani, F. (1995). Processi di estensione e circolazione di fluidi a bassa termalità nella Piana di Riardo (Caserta, Appennino centro-meridionale). *Bollettino della Societa Geologica Italiana*, *114*(2), 361–371.

Goldberg, A. S. (2010). Dyke swarms as indicators of major extensional events in the 1.9–1.2 Ga Columbia supercontinent. *Journal of Geodynamics*, *50*(3–4), 176–190. https://doi.org/10.1016/j.jog.2010.01.017

González, P. J. (2022). Volcano-tectonic control of Cumbre Vieja. *Science*, *375*(6587), 1348–1349. https://doi.org/10.1126/science.abn5148

Gudmundsson, A. (1983). Form and dimensions of dykes in eastern Iceland. *Tectonophysics*, *95*(3–4), 295–307. https://doi.org/10.1016/0040-1951(83)90074-4

Gudmundsson, A. (1984). Formation of dykes, feeder-dykes, and the intrusion of dykes from magma chambers. *Bulletin Volcanologique*, *47*(3), 537–550. https://doi.org/10.1007/bf01961225

Gudmundsson, A. (1990). Emplacement of dikes, sills and crustal magma chambers at divergent plate boundaries. *Tectonophysics*, *176*(3–4), 257–275. https://doi.org/10.1016/0040-1951(90)90073-h

Gudmundsson, A. (1992). Formation and growth of normal faults at the divergent plate boundary in Iceland. *Terra Nova*, *4*(4), 464–471. https://doi.org/10.1111/j.1365-3121.1992.tb00582.x

Gudmundsson, A. (2011). *Rock fractures in geological processes*. Cambridge University Press.

Gudmundsson, A. (2012). Magma chambers: Formation, local stresses, excess pressures, and compartments. *Journal of Volcanology and Geothermal Research*, *237*, 19–41. https://doi.org/10.1016/j.jvolgeores.2012.05.015

Gudmundsson, A. (2020). *Volcanotectonics: Understanding the structure, deformation and dynamics of volcanoes*. Cambridge University Press.

Hawkesworth, C. J., & Vollmer, R. (1979). Crustal contamination versus enriched mantle: $^{143}Nd/^{144}Nd$ and $^{87}Sr/^{86}Sr$ evidence from the Italian volcanics. *Contributions to Mineralogy and Petrology*, *69*(2), 151–165. https://doi.org/10.1007/bf00371858

Ippolito, F. (1973). Struttura marginale tirrenica dell'Appennino Campano: reinterpretazione di dati di antiche ricerche di idrocarburi.

Isaia, R., Vitale, S., Marturano, A., Aiello, G., Barra, D., Ciarcia, S., et al. (2019). High-resolution geological investigations to reconstruct the long-term ground movements in the last 15 kyr at Campi Flegrei caldera (southern Italy). *Journal of Volcanology and Geothermal Research*, *385*, 143–158. https://doi.org/10.1016/j.jvolgeores.2019.07.012

James, M. R., & Robson, S. (2012). Straightforward reconstruction of 3D surfaces and topography with a camera: Accuracy and geoscience application. *Journal of Geophysical Research*, *117*(F3), F03017. https://doi.org/10.1029/2011jf002289

Japan Aerospace Exploration Agency. (2021). ALOS World 3D 30-meter DEM. V3.2. Distributed by OpenTopography. https://doi.org/10.5069/G94M92HB

Jolis, E. M., Freda, C., Troll, V. R., Deegan, F. M., Blythe, L. S., McLeod, C. L., & Davidson, J. P. (2013). Experimental simulation of magma–carbonate interaction beneath Mt. Vesuvius, Italy. *Contributions to Mineralogy and Petrology*, *166*(5), 1335–1353. https://doi.org/10.1007/s00410-013-0931-0

Jolis, E. M., Troll, V. R., Harris, C., Freda, C., Gaeta, M., Orsi, G., & Siebe, C. (2015). Skarn xenolith record crustal CO_2 liberation during Pompeii and Pollena eruptions, Vesuvius volcanic system, central Italy. *Chemical Geology*, *415*, 17–36. https://doi.org/10.1016/j.chemgeo.2015.09.003

Knuever, M., Sulpizio, R., Mele, D., & Costa, A. (2023). Magma–rock interactions: A review of their influence on magma rising processes with emphasis on short-timescale assimilation of carbonate rocks. *Geological Society, London, Special Publications*, *520*(1), SP520–2021. https://doi.org/10.1144/sp520-2021-177

Koopmans, L., McCarthy, W., & Magee, C. (2022). Dyke architecture, mineral layering, and magmatic convection; new perspectives from the Younger Giant Dyke Complex, S Greenland. *Geochemistry, Geophysics, Geosystems*, *23*(3), e2021GC010260. https://doi.org/10.1029/2021gc010260

Le Bas, M., Maitre, R. L., Streckeisen, A., & Zanettin, B., & IUGS Subcommision on the Systematics of Igneous Rocks. (1986). A chemical classification of volcanic rocks based on the total alkali-silica diagram. *Journal of Petrology*, *27*(3), 745–750. https://doi.org/10.1093/petrology/27.3.745

Le Maitre, R. W., Streckeisen, A., Zanettin, B., Le Bas, M. J., Bonin, B., Bateman, P., et al. (2002). *Igneous rocks. A classification and glossary of terms: Recommendations of the international union of geological sciences subcommission on the systematics of igneous rocks* (Vol. 2). Cambridge University Press.

Lucci, F., Carrasco-Núñez, G., Rossetti, F., Theye, T., White, J. C., Urbani, S., et al. (2020). Anatomy of the magmatic plumbing system of Los Humeros Caldera (Mexico): Implications for geothermal systems. *Solid Earth*, *11*(1), 125–159. https://doi.org/10.5194/se-11-125-2020

Luhr, J. F., & Giannetti, B. (1987). The brown leucitic tuff of Roccamonfina Volcano (Roman region, Italy). *Contributions to Mineralogy and Petrology*, *95*(4), 420–436. https://doi.org/10.1007/bf00402203

Lustrino, M., Duggen, S., & Rosenberg, C. L. (2011). The Central-Western Mediterranean: Anomalous igneous activity in an anomalous collisional tectonic setting. *Earth-Science Reviews*, *104*(1–3), 1–40. https://doi.org/10.1016/j.earscirev.2010.08.002

Marra, F., Cardello, G. L., Gaeta, M., Jicha, B., Montone, P., Niespolo, E. M., et al. (2021). The Volsci Volcanic Field (central Italy): An open window on continental subduction processes. *International Journal of Earth Sciences*, *110*(2), 689–718. https://doi.org/10.1007/s00531-021-01981-6

Martelli, M., Nuccio, P. M., Stuart, F. M., Burgess, R., Ellam, R. M., & Italiano, F. (2004). Helium–strontium isotope constraints on mantle evolution beneath the Roman Comagmatic Province, Italy. *Earth and Planetary Science Letters*, *224*(3–4), 295–308. https://doi.org/10.1016/j.epsl.2004.05.025

Martinez-Poza, A. I., & Druguet, E. (2016). Structure and tectonic setting of the SE Sardinia mafic dyke swarm. Insights for the stress state during magma emplacement in the upper crust. *Journal of Geodynamics*, *101*, 170–185. https://doi.org/10.1016/j.jog.2016.05.012

Morgan, S., Stanik, A., Horsman, E., Tikoff, B., de Saint Blanquat, M., & Habert, G. (2008). Emplacement of multiple magma sheets and wall rock deformation: Trachyte Mesa intrusion, Henry Mountains. Utah. *Journal of Structural Geology*, *30*(4), 491–512. https://doi.org/10.1016/j.jsg.2008.01.005

Natale, J. (2023). The Taverna San Felice dike (NE of Roccamonfina volcano): Unravelling magmatic intrusion processes and volcano-tectonics in the Tyrrhenian margin of the southern Apennines. [Dataset]. https://doi.org/10.17605/OSF.IO/PC2YE

Natale, J., Camanni, G., Ferranti, L., Isaia, R., Sacchi, M., Spiess, V., et al. (2022). Fault systems in the offshore sector of the Campi Flegrei caldera (southern Italy): Implications for nested caldera structure, resurgent dome, and volcano-tectonic evolution. *Journal of Structural Geology*, *163*, 104723. https://doi.org/10.1016/j.jsg.2022.104723

Nicotera, P., & Civita, M. (1969). Ricerche idrogeologiche per la realizzazione delle opere di presa delle sorgenti Mercato e Palazzo in Sarno (Campania). *Memorie e Note Istituto Geologia Applicata Napoli*, *13*.

Open Stereo Sofware Package. (2018). Retrieved from https://github.com/endarthur/os/releases/latest

Peccerillo, A. (2017). *Cenozoic volcanism in the Tyrrhenian Sea Region, advances in volcanology*. Springer International Publishing AG. https://doi.org/10.1007/978-3-319-42491-0

Pollard, D. D., & Segall, P. (1987). Theoretical displacements and stresses near fractures in rocks: With applications to faults, joints, veins, dikes, and solution surfaces. In B. K. Atkinson (Ed.), *Fracture mechanics of rock* (pp. 277–349). Academic Press.

Poppe, S., Galland, O., de Winter, N. J., Goderis, S., Claeys, P., Debaille, V., et al. (2020). Structural and geochemical interactions between magma and sedimentary host rock: The Hovedøya case, Oslo Rift, Norway. *Geochemistry, Geophysics, Geosystems*, *21*(3), e2019GC008685. https://doi.org/10.1029/2019GC008685

Porreca, M., Acocella, V., Massimi, E., Mattei, M., Funiciello, R., & De Benedetti, A. A. (2006). Geometric and kinematic features of the dike complex at Mt. Somma, Vesuvio (Italy). *Earth and Planetary Science Letters*, *245*(1–2), 389–407. https://doi.org/10.1016/j.epsl.2006.02.027

Reiter, F., & Acs, P. (1996-2020). TectonicsFP ©1996-2020 help version 1.7.14.

Rouchon, V., Gillot, P. Y., Quidelleur, X., Chiesa, S., & Floris, B. (2008). Temporal evolution of the Roccamonfina volcanic complex (Pleistocene), Central Italy. *Journal of Volcanology and Geothermal Research*, *177*(2), 500–514. https://doi.org/10.1016/j.jvolgeores.2008.07.016

Ruch, J., Wang, T., Xu, W., Hensch, M., & Jónsson, S. (2016). Oblique rift opening revealed by reoccurring magma injection in central Iceland. *Nature Communications*, *7*(1), 12352. https://doi.org/10.1038/ncomms12352

Russo Ermolli, E., Aucelli, P. P., Di Rollo, A., Mattei, M., Petrosino, P., Porreca, M., & Rosskopf, C. M. (2010). An integrated stratigraphical approach to the Middle Pleistocene succession of the Sessano basin (Molise, Italy). *Quaternary International*, *225*(1), 114–127. https://doi.org/10.1016/j.quaint.2009.04.008

Santello, L. (2010). Analysis of a trampled formation: The Brown Leucitic Tuff (Roccamonfina volcano, Southern Italy).

Scudero, S., De Guidi, G., & Gudmundsson, A. (2019). Size distributions of fractures, dykes, and eruptions on Etna, Italy: Implications for magma-chamber volume and eruption potential. *Scientific Reports*, *9*(1), 4139. https://doi.org/10.1038/s41598-019-40563-0

Servizio Geologico d'Italia. (1968). Geological map of Italy, scale 1: 100,000, sheet 171 Gaeta.

Sgrosso, I., & Aiello, R. (1963). Bocca eruttiva presso Presenzano (Caserta). *Bollettino della Società Naturalisti in Napoli*, 72.

Smets, B., Kervyn, M., d'Oreye, N., & Kervyn, F. (2015). Spatio-temporal dynamics of eruptions in a youthful extensional setting: Insights from Nyamulagira Volcano (DR Congo), in the western branch of the East African Rift. *Earth-Science Reviews*, *150*, 305–328. https://doi.org/10.1016/j.earscirev.2015.08.008

Smith, I. E. M., & Németh, K. (2017). Source to surface model of monogenetic volcanism: A critical review. *Geological Society, London, Special Publications*, *446*(1), 1–28. https://doi.org/10.1144/sp446.14

Stimac, J., Goff, F., & Goff, C. J. (2015). Intrusion-related geothermal systems. In *The encyclopedia of volcanoes* (pp. 799–822). Academic Press.

Streck, M. J. (2008). Mineral textures and zoning as evidence for open system processes. *Reviews in Mineralogy and Geochemistry*, *69*(1), 595–622. https://doi.org/10.2138/rmg.2008.69.15

Štroner, M., Urban, R., Seidl, J., Reindl, T., & Brouček, J. (2021). Photogrammetry using UAV-mounted GNSS RTK: Georeferencing strategies without GCPs. *Remote Sensing*, *13*(7), 1336. https://doi.org/10.3390/rs13071336

Tedesco, C. (1965). Main lines of the history of the Roccamonfina volcano. *Bulletin Volcanologique*, *28*(1), 119–137. https://doi.org/10.1007/bf02596920

Tibaldi, A., Bonali, F. L., Russo, E., & Fallati, L. (2020). Surface deformation and strike-slip faulting controlled by dyking and host rock lithology: A compendium from the Krafla Rift, Iceland. *Journal of Volcanology and Geothermal Research*, *395*, 106835. https://doi.org/10.1016/j.jvolgeores.2020.106835

Tramparulo, F. D. A., Vitale, S., Isaia, R., Tadini, A., Bisson, M., & Prinzi, E. P. (2018). Relation between alternating open/closed-conduit conditions and deformation patterns: An example from the Somma-Vesuvius volcano (southern Italy). *Journal of Structural Geology*, *112*, 138–153. https://doi.org/10.1016/j.jsg.2018.05.008

Trippanera, D., Ruch, J., Acocella, V., & Rivalta, E. (2015). Experiments of dike-induced deformation: Insights on the long-term evolution of divergent plate boundaries. *Journal of Geophysical Research: Solid Earth*, *120*(10), 6913–6942. https://doi.org/10.1002/2014jb011850

Trippanera, D., Ruch, J., Acocella, V., Thordarson, T., & Urbani, S. (2018). Interaction between central volcanoes and regional tectonics along divergent plate boundaries: Askja, Iceland. *Bulletin of Volcanology*, *80*, 1–19. https://doi.org/10.1007/s00445-017-1179-8

Trippanera, D., Ruch, J., Passone, L., & Jónsson, S. (2019). Structural mapping of dike-induced faulting in Harrat Lunayyir (Saudi Arabia) by using high resolution drone imagery. *Frontiers in Earth Science*, *7*, 168. https://doi.org/10.3389/feart.2019.00168

USGS. (2017). USGS national UAS project office. Unmanned aircraft systems data post-processing: Structure-from-motion photogrammetry. Retrieved from https://uas.usgs.gov/nupo/pdf/USGSAgisoftPhotoScanWorkflow.pdf

Valente, E., Buscher, J. T., Jourdan, F., Petrosino, P., Reddy, S. M., Tavani, S., et al. (2019). Constraining mountain front tectonic activity in extensional setting from geomorphology and Quaternary stratigraphy: A case study from the Matese ridge, southern Apennines. *Quaternary Science Reviews*, *219*, 47–67. https://doi.org/10.1016/j.quascirev.2019.07.001

Vitale, S., & Ciarcia, S. (2013). Tectono-stratigraphic and kinematic evolution of the southern Apennines/Calabria–Peloritani Terrane system (Italy). *Tectonophysics*, *583*, 164–182. https://doi.org/10.1016/j.tecto.2012.11.004

Vitale, S., & Ciarcia, S. (2018). Tectono-stratigraphic setting of the Campania region (southern Italy). *Journal of Maps*, *14*(2), 9–21. https://doi.org/10.1080/17445647.2018.1424655

Vitale, S., & Ciarcia, S. (2022). The dismembering of the Adria platforms following the Late Cretaceous-Eocene abortive rift: A review of the tectono-stratigraphic record in the southern Apennines. *International Geology Review*, *64*(20), 2866–2889. https://doi.org/10.1080/00206814.2021.2004559

Vitale, S., & Isaia, R. (2014). Fractures and faults in volcanic rocks (Campi Flegrei, southern Italy): Insight into volcano-tectonic processes. *International Journal of Earth Sciences*, *103*(3), 801–819. https://doi.org/10.1007/s00531-013-0979-0

Vitale, S., Isaia, R., Ciarcia, S., Di Giuseppe, M. G., Iannuzzi, E., Prinzi, E. P., et al. (2019). Seismically induced soft-sediment deformation phenomena during the volcano-tectonic activity of Campi Flegrei caldera (southern Italy) in the last 15 kyr. *Tectonics*, *38*(6), 1999–2018. https://doi.org/10.1029/2018tc005267

Vitale, S., Prinzi, E. P., Tramparulo, F. D. A., De Paola, C., Di Maio, R., Piegari, E., et al. (2020). Late Miocene-early Pliocene out-of-sequence thrusting in the southern Apennines (Italy). *Geosciences*, *10*(8), 301. https://doi.org/10.3390/geosciences10080301

Vollmer, R. (1976). Rb-Sr and U-Th-Pb systematics of alkaline rocks: The alkaline rocks from Italy. *Geochimica et Cosmochimica Acta*, *40*(3), 283–295. https://doi.org/10.1016/0016-7037(76)90205-2

Vollmer, R., & Hawkesworth, C. J. (1980). Lead isotopic composition of the potassic rocks from Roccamonfina (South Italy). *Earth and Planetary Science Letters*, *47*(1), 91–101. https://doi.org/10.1016/0012-821x(80)90107-7

Weismüller, C., Urai, J. L., Kettermann, M., von Hagke, C., & Reicherter, K. (2019). Structure of massively dilatant faults in Iceland: Lessons learned from high-resolution unmanned aerial vehicle data. *Solid Earth*, *10*(5), 1757–1784. https://doi.org/10.5194/se-10-1757-2019

Westerman, D., Rocchi, S., Breitkreuz, C., Stevenson, C., & Wilson, P. (2017). Structures related to the emplacement of shallow-level intrusions. In C. Breitkreuz & S. Rocchi (Eds.), *Physical geology of shallow magmatic systems. Advances in volcanology*. Springer, Cham. https://doi.org/10.1007/11157_2017_31